[Mechanisms for anomalous organic matter concentrations within the Roseneath-Epsilon-Murteree section of the Cooper Basin]

Thesis submitted in accordance with the requirements of the University of Adelaide for an Honours Degree in Geology/Geophysics/Environmental Geoscience

Troy Granger

November 2013

THE UNIVERSITY
of ADELAIDE

MECHANISMS FOR ANOMALOUS ORGANIC MATTER CONCENTRATIONS WITHIN THE ROSENEATH-EPSILON-MURTEREE SECTION OF THE COOPER BASIN

ABSTRACT

2- 8% organic carbon enrichment within the Permian Roseneath-Epsilon-Murteree (REM) interval, deposited in a post glacial, cold climate system, goes against many well established paradigms for viable source rock deposition. Understanding the source of organic matter and the timing of diagenesis within this system may shed light onto the viability of this and other cold climate depositional systems as hydrocarbon source rock domains. The dominant lithology of the REM, based on core observations, backscattered electron microscopy (BSEM) and X-ray Diffraction (XRD), indicates a compositionally immature greywacke containing ~40% quartz, ~20% mica, and ~40% diagenetic products (kaolinite, illite, siderite and minor chlorite). BSEM highlights 2 dominant organic matter forms: 20-50μm particles with defined tabular and spherical shapes, and intergranular pore residing organics with grain coating features. RockEval indicates low S2 values varying between 0.1 and 3.0mgHC/gTOC indicative of low generative potential. Diagenetic kaolinite, illite, chlorite and Fe rich and Mg rich phases of siderite occlude the bulk of intergranular porosity. Variations in siderite abundance track coarser siltstone laminations on the 1-5mm scale, occurring as bands visible at the micron and core scale. Replacement of detrital mica and diagentic illite by siderite is observed in BSEM, while stable phases of kaolinite are observed in both Vintage Crop 1 (minimum %Ro=0.76) and Encounter 1 (minimum %Ro=3.6). The dominance of detrital plant material, the presence of pore-filling, grain coating organics, and the low generative potential of REM organics implies a migration driven hydrocarbon system. The key to prospectivity in the REM may therefore be linked to the timing of diagenetic pore filling seals relative to charge migration as opposed to in situ hydrocarbon generation.

KEYWORDS

2

Table of Contents

LIST OF FIGURES AND TABLES

INTRODUCTION

Within the stratigraphic record, there is a marked bias with regards to deposition of organic rich material in greenhouse Earth conditions (Arthur & Schlanger 1979, Weissert & Mohr 1996). A review of source rocks around the globe by Klemme and Ulmishek (1991) indicated that approximately 60% of exploited oil and gas reserves were derived from organic rich rocks (ORRs) deposited in greenhouse Earth conditions between the late Jurassic and middle Cretaceous. Within the ancient and modern sediment record, there is also prevalence towards source rock development within low latitude marine continental margin settings, where high productivity and anoxic bottom waters promote deposition and preservation of organic matter (Hedges & Keil 1995). In fact, preserved organic matter within sedimentary rocks from continental margin settings accounts for approximately 43 percent of all carbon buried (Berner & Canfield 1989).

Nonetheless, coal and lacustrine source rocks capable of hydrocarbon generation are not uncommon. Lacustrine shales from the Eocene Green River Formation in the US is well documented as a source rock in low maturity systems (Tissot *et al.* 1978, Horsfield *et al.* 1994, Carroll & Bohacs 2001), while in China, commercial scale exploitation of hydrocarbons from both Tertiary and Upper Triassic-Middle Jurassic lacustrine shales and coal measures occurs in numerous basins (Graham *et al.* 1990, Ritts *et al.* 1999). However, these systems again record deposition during greenhouse intervals, reinforcing a link between warmer climates and source rock abundance.

A need to better understand the fundamental processes involved in carbon burial within fine grained sediments has been a recent focus within the scientific community, driven largely by successful shale gas exploitation in North America. This is the result of technological advancement in horizontal drilling and hydraulic fracturing techniques and has made organic rich shale both a source of hydrocarbons and a reservoir, greatly simplifying the hydrocarbon system by eliminating the migration, seals and trap (Zahid *et al.* 2007). Self sourced shales now account for almost a quarter of total natural gas production in America (EIA 2011).

In Australia, shale gas has been most widely promoted within the Cooper Basin, where significant gas shows have been reported in the Permian section in the Nappamerri Trough (Hill *et al.* 2011). While contention exists as to whether gas within the Roseneath-Epsilon-Murteree (REM) section in the Nappamerri is self-sourced, or is part of a larger basin centred gas accumulation (Hillis *et al.* 2001), the presence of organic matter within what is ordinarily a markedly different environment for organic matter development and preservation remains noteworthy. Basin development occurred in an intracratonic setting with a strong tectonic influence not only on sediment sourcing but also climate (Veevers 2006). Deposited in the waning stages of glaciations, at mid to high latitudes in a cold to temperate climate, the Cooper Basin source rocks are dominated by Permian coal packages present within the Gidgealpa Group (Alexander *et al.* 1998). Carbonaceous shales and silts are also prevalent in a number of units within the Gidgealpa Group, but are particularly extensive within the lacustrine Roseneath and Murteree Shales of the REM interval, with total organic carbon (TOC) values as high as 5% recorded previously (Hill *et al.* 2011). Given the cold climate and tectonically active

environment within which the REM was deposited, what accounts for the carbon deposition and preservation that is so widespread within this interval?

A number of mechanisms are suggested to explain organic matter deposition and preservation within marine and lacustrine environments. Traditionally, oceanic and lacustrine organic carbon variations have been attributed to dilution by sediment influx (Lindsay 2000, Tyson 2001, Sageman *et al.* 2003), fluxes in organic matter driven by organism productivity and terrigenous input (Isaacs 1987, Emerson & Hedges 1988, Smith & Bustin 1998), and minimised oxidation through depleted oxygen conditions (Rimmer et al 2004, Arthur and Sageman 1994). The relative rates of dilution, production and destruction are argued to account for almost all variation in the abundance of organic matter within deposited sediments (Tyson 2001, Bohacs *et al.* 2005, Passey *et al.* 2010). In lacustrine systems like those in which the Roseneath and Murteree shales were deposited, organic matter is principally derived from algal matter and detrital vascular plant material (Meyers & Ishiwatari 1993). Fluxes in algal matter are particularly common in large, thermally stratified lakes where there is seasonal overturn. Organic matter deposited by this mechanism is typically cyclically laminated and have high hydrogen indexes. Detrital vascular plant material conversely would show lower hydrogen index values. Material of this form should have consistent, well defined shapes indicative of the plant materials they are derived from.

Alternatively, organic preservation effects of mineral surfaces has been shown to play an important role in black shale deposits, with studies showing a quantitative relationship between mineral surface area (MSA) and TOC (Keil *et al.* 1994, Mayer

1994, Ransom *et al.* 1998, Kennedy *et al.* 2002, Pearson *et al.* 2002, Kennedy & Wagner 2011). Many of these studies focus on high surface area clay minerals of the smectite family, which typically form in warm or seasonal environments where chemical weathering is extensive in soils (Boeglin & Probst 1998, Wilson 1999, Thiry 2000), or during the breakdown of volcanics (Cole & Shaw 1983). As these weathering conditions are unlikely in glacial environments in the Permian during the deposition of the REM interval, this pathway to carbon preservation seems unlikely. However, clay minerals of some origin are present in the REM interval, and need to be accounted for.

While mechanisms have been posed for deposition and preservation of a primary form organic matter, potential also exists that organic matter present within the REM is not of primary origin. Reworked lithified organic matter in the form of earlier deposited shales and coals could provide a source of organic carbon that would be resistant to breakdown and degradation. Such an OM form would likely be represented by large, well defined lithic fragments with extremely low hydrogen indexes. Alternatively, organic carbon may have migrated into the system as hydrocarbon and become trapped, though this is unlikely to represent the bulk of OM within the widespread REM. For this mechanism, evidence of oil staining would be expected, as well as grain coating textures at the micron scale.

Utilising a combination of multiscale optical analyses, surface area analysis, pyrolysis induced artificial maturation studies (RockEval), and carbon isotope analysis, this study will test the hypothesis that organic matter preservation within the REM is driven by

seasonally driven influxes of reworked refractory organic matter such as coals and shales, more resistant to oxidation, and is not a primary depositional product.

GEOLOGICAL SETTING/BACKGROUND

The Cooper Basin is an intracratonic, non-marine basin encompassing approximately 153,000 square kilometres within Queensland, South Australia and part of New South Wales (Alexander *et al.* 1998). The Cooper basin unconformably overlies the Warburton Basin, and is unconformably overlain by the Eromanga Basin.

The sedimentary deposits within the Cooper Basin are divided into two separate groups: The non-marine, glacial Late Carboniferous to Permian sediments of the Gidgealpa Group and the Late Permian to Mid Triassic marine sediments of the Nappamerri Group (Alexander *et al.* 1998, Smith & Griffiths 1999). The Roseneath Shale, Epsilon Formation and Murteree Shale (REM) (Figure 1), the principle formations of focus for this study, are found within the Gidgealpa Group sediments. Also within the Gidgealpa Group is the Patchawarra Formation, which conformably underlies the Murteree Shale. Coals within the Patchawarra Formation have long been considered a major source of hydrocarbons within the Cooper Basin (Alexander *et al.* 1998).

The Cooper Basin can also be divided spatially into the Patchawarra, Nappamerri, Tenappera and Allunga Troughs, separated by a series of northeast trending syn-sedimentary asymmetric ridges that are often arcuate in nature and are bound to the north and south by faulting (Mavromatidis 2008). The two deepest, most widely studied and most economically exploited of these troughs, the Patchawarra and Nappamerri troughs (Figure 2), are separated by the Gidgealpa-Merrimelia-Innamincka (GMI) anticlinal trend (Kuang 1985). The Nappamerri Trough, a current target for shale gas, is the deepest trough within the Cooper Basin and has the thickest sediment accumulations (Alexander *et al.* 1998).
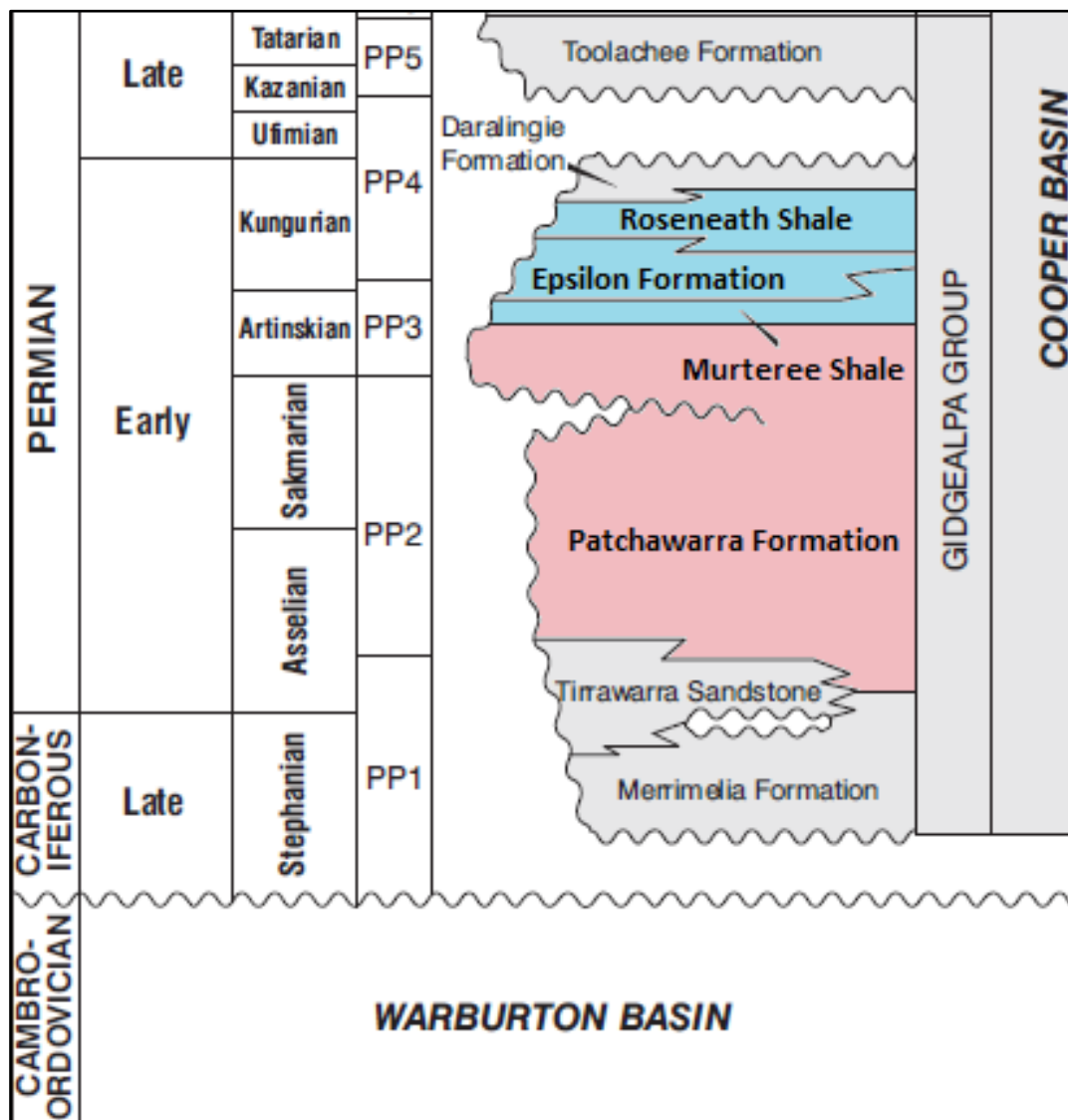
Figure 1: Stratigraphic column of the Warburton basin and overlying Gidgealpa Group of the Cooper Basin. The focus of this study, the Early Permian Roseneath-Epsilon-Murteree formations, are highlighted blue, while the Patchawarra Formation, containing major hydrocarbon sourcing coals, is highlighted pink (modified after Alexander *et al.* 1998)
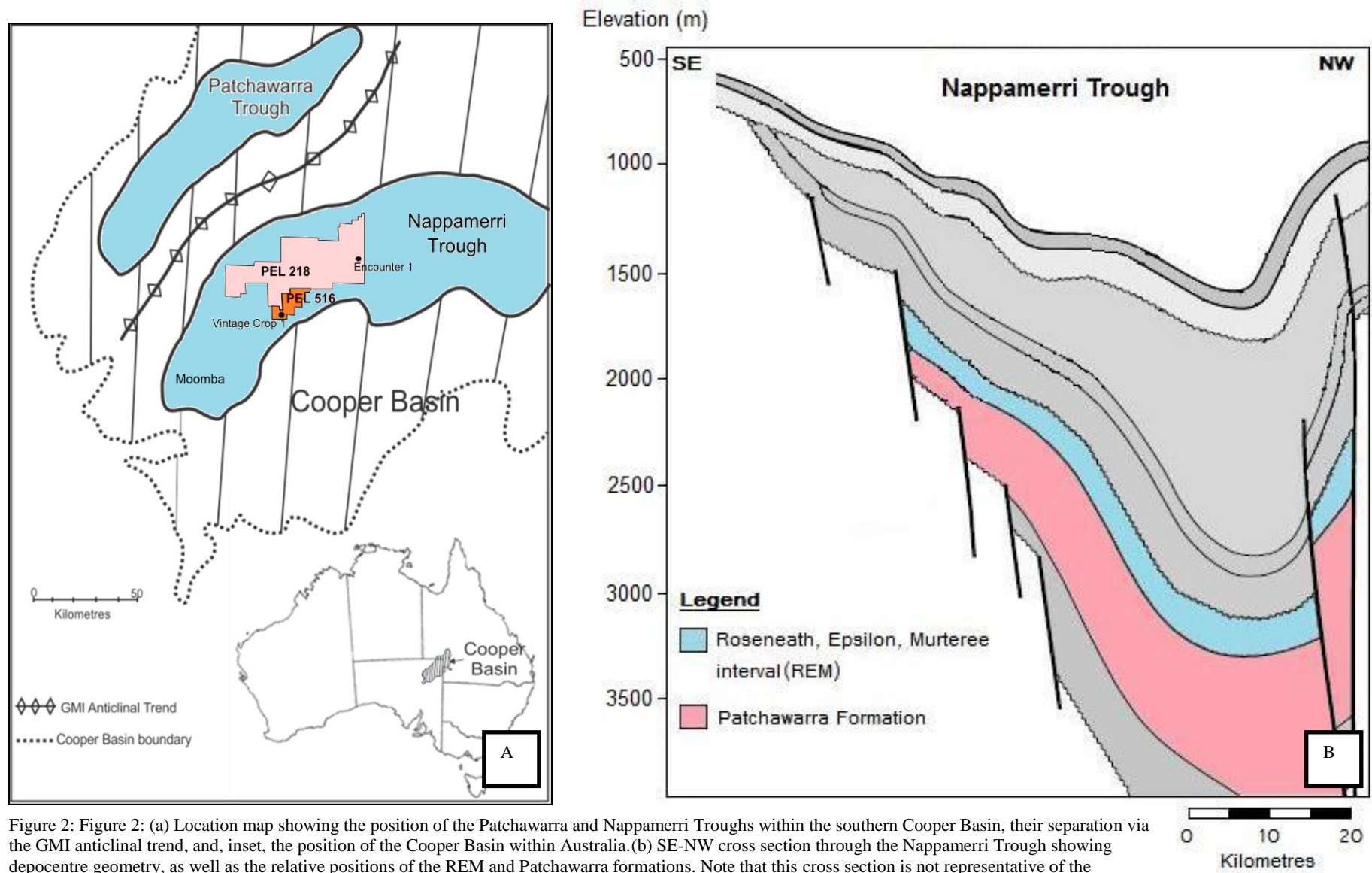
Figure 2: Figure 2: (a) Location map showing the position of the Patchawarra and Nappamerri Troughs within the southern Cooper Basin, their separation via the GMI anticlinal trend, and, inset, the position of the Cooper Basin within Australia.(b) SE-NW cross section through the Nappamerri Trough showing depocentre geometry, as well as the relative positions of the REM and Patchawarra formations. Note that this cross section is not representative of the maximum depth reached within the Nappamerri Trough.

REM Stratigraphy

Table 1: Stratigraphic descriptions of the Roseneath-Epsilon-Murteree formations, including age constraints based on palynology and interpreted depositional environment. Sediments within the Roseneath-Epsilon-Murteree formations are not present as outcropping units, meaning that information regarding their lithology, mineralogy, unit contacts and geomorphologies are derived entirely from seismic data, drill core and rock chip analyses.

Unit	Age of deposition based on palynology(Price et al 1985)	Unit Boundary contacts	Description	Interpreted Sedimentary Environment (Alexander *et al.* 1998).
Roseneath Shale	Kungurian (279-272)	The Roseneath Shale conformably overlies the fluvial sandstones of Epsilon Formation and is overlain by sandstone and mudstones of the Daralingie Formation.	The Roseneath Shale comprises dominantly siltstone varying in colour from light to dark brown, interbedded with mudstone and minor fine pale brown sands (Gatehouse 1972, Kapel 1972, Thornton & Hudson 1979). The Roseneath Shale is prevalent across much of the central Cooper Basin, reaching a maximum thickness of 100m around the Nappamerri and Tennapera troughs (Alexander *et al.* 1998). On crests and ridges such as the Dunoon and Murteree ridges, the Roseneath section has been eroded. Silt beds within the Roseneath Shale vary from massive to finely laminated and rhythmic, can be carbonaceous and are often micromicaceous, also containing minor fine grained disseminated pyrite likely diagenetic in origin (Gatehouse 1972, Kapel 1972, Thornton & Hudson 1979). Soft sediment features such as slumps, load marks and flame structures are common, while rare wavy ripples indicative of storm reworking may also be present.	Broad, deep fresh water lake
Epsilon Formation	Artinskian (290-279 Ma)to Kungarian (279-272Ma)	The Epsilon Formation conformably overlies the Murteree Shale and is conformably	The Epsilon Formation comprises thinly bedded quartz rich sands interbedded with dark grey-brown carbonaceous siltstone and shale, as well as coal (Gatehouse 1972, Kapel 1972, Thornton & Hudson 1979). It is widespread across the central Cooper Basin and reaches a maximum thickness of 156m within the Nappamerri Trough, however is not present on structural highs due to erosion (Alexander *et al.* 1998). The Epsilon Formation can be divided into 3 sediment packages representing differing depositional environments: (1) The basal depositional stage comprises upward coarsening siltstone grading into ripple	(1) Lacustrine delta fill (2) Swamp and prograding delta plain (3) Fluvial

		overlain by the Roseneath Shale.	and planar bedded sandstones. (2) Thick coal rich package and ribbon sandstones, where coal seams vary from 2-20m in thickness (3) Upward coarsening sandstones with low angle bedding, minor trough cross lamination and characteristic bioturbation and soft sediment deformation features.	
Murteree Shale	Artinskian (290-279 Ma)	The Murteree Shale conformably overlies the Patchawarra Formation, and is conformably overlain by the Epsilon Formation.	The Murteree Shale dominantly comprises horizontally and at times rhythmically laminated black to dark grey siltstone with fine sandstone interbeds, containing a higher proportion of sand to the south (Gatehouse 1972, Kapel 1972, Thornton 1979, Williams 1995). Siltstones may be carbonaceous, and often contain fine grained pyrite and muscovite. It is the most widespread formation of the REM units, occurring across much of the Cooper Basin in both South Australia and Queensland and at an average thickness of approximately 50m. However, like the Roseneath and Epsilon formations, the Murteree Shale is thickest in the Nappamerri Trough (~80m thick), and has been eroded from structural highs (Alexander *et al.* 1998). The siltstones within the Murteree shale show minor lenticular bedding, as well as rare wave ripples. Occasional turbidite sequences may also be observed, as may rare dropstones. Slump folding, microfaults and bioturbation are common features.	Broad, deep fresh water lake

Tectonic and climate influence on REM deposition

10 million years prior to the initial development of the Cooper Basin, during the Late to Mid Carboniferous, the region was dominated by high heat flow and granite emplacement, as well as uplift in central Australia attributed to the Kanimblan and Alice Springs orogenies (Veevers 2006). These periods of orogenisis are thought to be a product of stress propagation from the Eastern Australian plate margin as a result of collision between Gondwana and Laurasia during the formation of Pangea (Powell & Veevers 1987). A recorded change from carbonate and evaporate deposits to those dominated by glacial, detrital and coal sequences has been used to imply a change in latitude from equatorial to one that was much higher (~70° S)(Veevers 2006). The tectonically driven increase in altitude in combination with the paleolatitude of Australia resulted in glaciation, evident in striated pavements and stones, glendonites, tillites and dropstones present in Permian aged deposits of South Australia (Crowell & Frakes 1971). U-Pb dating of detrital zircons from Eastern Australian glacial deposit facies suggests ice sheet development occurred in the mid to late Carboniferous (Veevers 2006).

Glacial retreat was prevalent in the Early Permian, as a result of the drift of Australia to lower latitudes (Alexander *et al.* 1998). The temperate climate along with intermittent high sediment influx associated with ice sheet melting and continued regional subsidence led to the deposition of intermittent fluvial to fluvio-lacustrine conditions interbedded with peat swamps and flood plains. The Patchawarra Formation, deposited during the Asselian to Artinskian, contains sinuous fluvial system facies dominated by coarse sands interbedded with overbank silts, shales and coals (Alexander *et al.* 1998).

The Artinskian through to the Kungurian was a period of relative tectonic stability, characterised by widespread deposition of the Murteree, Epsilon, and Roseneath formations (Kuang 1985). The environment of deposition for the Murteree, Epsilon and Roseneath formations is one of fluctuation between dominantly lacustrine (as for the Murteree and Roseneath Formations) and fluvial deltaic environments (for the Epsilon Formation) (Alexander *et al.* 1998).

METHODS

Samples were collected from Encounter 1 and Vintage Crop 1 cores, stored at DMITRE core library, South Australia. Both cores intersect the REM interval within the Nappamerri Trough (Figure 2, a); however at different depths reflected in their differing thermal maturities (Table 1). Encounter 1 and Vintage Crop 1 were studied to ascertain the lithological, geochemical and diagenetic variability not only over a thermal gradient, but also for differing basinal positions. Cores were logged for lithology, sedimentary structures and diagenetic features, and then sampled for a variety of geochemical, petrophysical and isotopic analyses (detailed below).

Table 2: Summary of key well information for Vintage Crop 1 and Encounter 1, taken from Vintage Crop 1 and Encounter 1 well completion reports.

Core	Vintage Crop 1	Encounter 1
Petroleum Exploration Licence	516	218
Latitude	28˚ 30' 29.24˚S	27˚ 45' 16.6554˚S
Longitude	140˚ 41' 38.09˚E	140˚ 57' 30.6957˚E
Section of REM missing?	Epsilon Formation	None missing
Depth of core sampled	1840-1960m	3266-3542m
Approximate Maturity (Ro)	0.8-0.9%	3-4%

Geochemical Analysis

124 sub-samples were cleaned, dried and milled to a fine powder for a variety of geochemical analyses (detailed further in Appendix A). 32 subsamples from a 15cm continuous section within the Vintage Crop 1 Roseneath shale were taken for analysis at approximately 5mm intervals.

 Total carbon was measured using a Perkin Elmer Series II CHNS/O Analyser 2400, and inorganic carbon content was established using the pressure calcimeter method set forth by Sherrod *et al.* (2002). Total organic carbon was calculated using the following equation:

Total Organic Carbon (%) = Total Carbon (%) − Inorganic Carbon (%)

To determine maturity and generative potential (S2) variation, pyrolysis induced artificial maturation of organics were conducted by Trican Well Solutions using methodologies based on the RockEval method set forth by Espitalie *et al.* (1977). Mineral Surface Area (MSA) was determined using Ethylene Glycol Monoethyl Ether (EGME) based on the 'free surface method' procedure of Tiller and Smith (1990), and given as silicate mineral surface area in metres squared per gram (m^2/g) on an organic carbon and carbonate free basis. 10 high TOC subsamples were treated with sodium hypochlorite to remove organic matter and again tested for MSA to determine organic matter influence on surface area calculations.

Bulk powder mineralogy of selected representative samples was examined using X-ray diffraction (XRD) on a Bruker D8 Advance XRD with a Cu radiation source. Bruker DIFRAC.EVA software and Crystallography Open Database reference patterns were used to assign peaks to specific mineral phases. A further 10 samples were selected for

clay fraction XRD, and treated with acetic acid and sodium hypochlorite to remove the carbonate and organics. The <2 micron clay fraction was placed onto silicon wafers for clay fraction XRD analysis. Mineral identification was performed on air dried and ethylene glycol (EG) treated samples, using the USGS Clay Mineral Identification Flow Diagram by Poppe *et al.* (2001).

Petrophysical Analyses

Thin section and scanning electron microscope (SEM) analyses were conducted on selected samples to examine variations in sediment composition, porosity and diagenetic alteration.. Representative thin sections were prepared by Prograding Rock Services and Pontifex & Associates Ltd for viewing using reflected and transmission light optical petrography on a Nikkon LV100 POL microscope. Backscattered scanning electron microscopy was conducted on polished blocks using the FEI Quanta 450 scanning electron microscope. 2 Subsamples were selected for electron microprobe analysis using the Cameca SX51 at Adelaide Microscopy, to ascertain relationships between deposition and diagenetic alteration.

Isotopic Analyses

Stable isotope analyses were conducted on 8 powdered Vintage Crop samples of varying siderite abundance by the University of Melbourne using continuous-flow isotope-ratio mass spectrometry on an Analytical Precision AP2003, which carries a precision of +/- 0.1 per mil for oxygen and +/- 0.05 per mil for carbon. Samples were digested in 105% phosphoric acid at 70°C and mass spectrometric measurements were made on the evolved CO2 gas. Results were normalised to the Vienna Pee Dee

Belemnite scale using internal working standards of Carrara Marble (NEW1 –

Newcastle), and cross-checked against the international standards NBS18 and NBS19.

OBSERVATIONS AND RESULTS

Lithological observations

The Roseneath and Murteree Shales are dominated by planar, rhythmically

interlaminated organic rich and siderite stained siltstone layers (Figure 3, a, b),

particularly prevalent within the Roseneath Shale of Vintage Crop 1 and widespread

throughout the Roseneath and Murteree shales in Encounter 1. These rhythmic layers

vary in thickness from 1mm up to 2cm. At unmagnified visual scales, there is no grain

size difference between the organic rich siltstone bands and those stained with siderite,

though finer scaled imaging indicates otherwise (see below). Lobes of wavy, silt to fine

sand dominated rippled lobes are present within the Roseneath and Murteree shales

(Figure 4, a), commonly near formation boundaries, which indicates an influence from

tractional currents as opposed to pelagic settling. Intermittent coarse sandy quartz rich

lag (1-3cm thick) forms scours that cut into the underlying laminations throughout each

core (Figure 4, b). These scours likely represent density flows. Siltstone intraclasts up to

2cm in size occur commonly throughout the Roseneath and Murteree, indicating local

reworking of unlithified sediments. Rare fragments of coaly organic matter (1mm-5mm)

are also apparent throughout both Vintage Crop 1 and Encounter 1 cores.
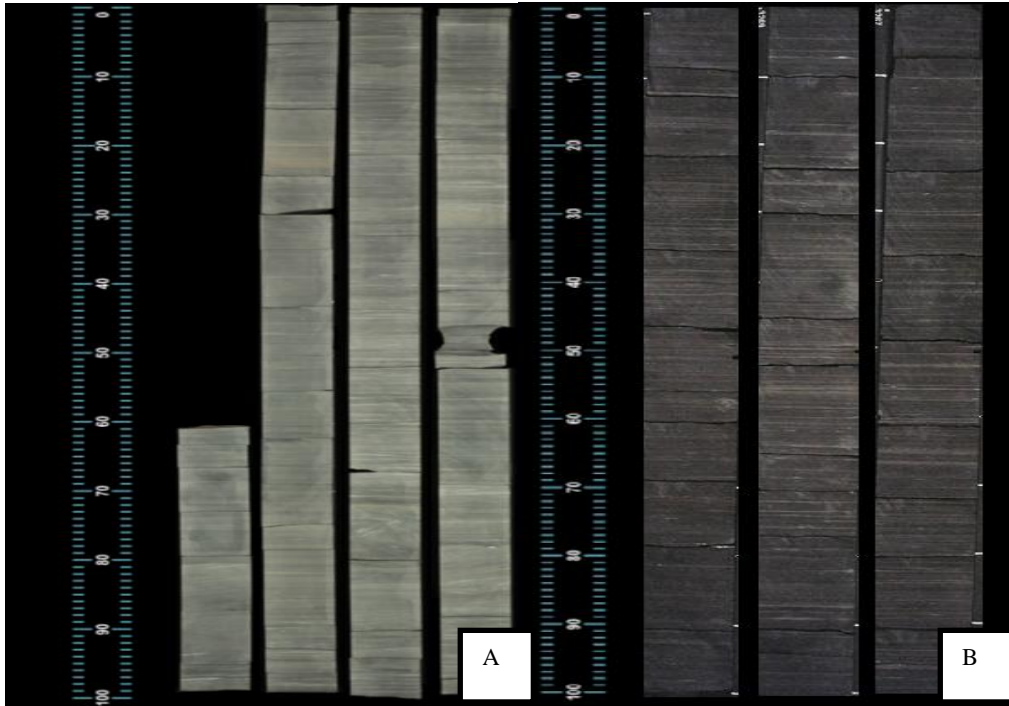
Figure 3: Photographs from selected sections from (a) Vintage Crop 1 (b) and Encounter 1 cores, illustrating the planar, rhythmic laminations present within sections of the Roseneath and Murteree shales.
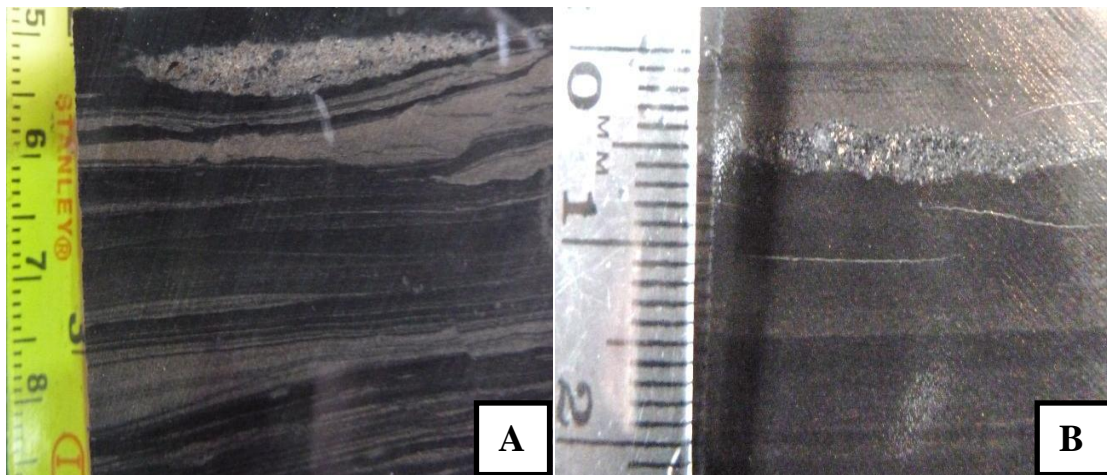
Figure 4: Core photographs indicating higher energy inputs within the Roseneath and Murteree shales. (a) Lobes of silt and fine sand are interbedded with carbonaceous fine silt laminations. Truncation and pinch outs features are apparent, as is microfaulting within the sandy intervals. A coarse sandy lag at the top of the image is cutting into the underlying siltstone. (b) Coarse sandy lag cutting into underlying dark siltstone. A gradation in colour from the coarse lag into light grey and then darker laminations is apparent at a scale of 5mm.

Zones with pervasive siderite precipitation are common, occurring both as packages of fine (1-5mm) orange to red sideritic laminations that constitute sequences up to 15cm thick (Figure 5, a) and as nodular concretions that vary in size from a few millimetres up to as large as 10cm (Figure 5, b).
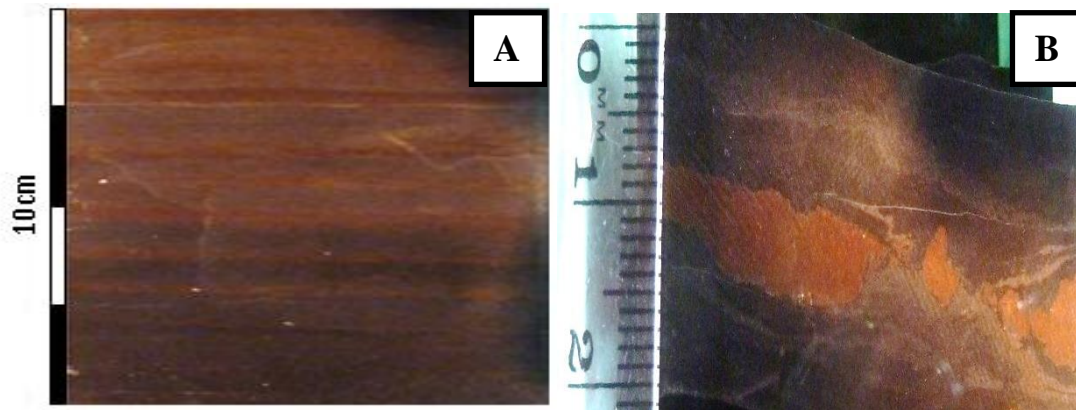
Figure 5: Photographs from Vintage Crop 1 indicating the nature of siderite development within the REM in core sample. (a) The Rosenaeth Shale (depth=1848.2m) showing siderite developing as packages of cyclic bands ~5mm thick, that appear to grade upward. (b) The Roseneath Shale (depth=1853.8m) showing 0.5-1 cm sideritic nodules present within a carbonaceous fine silt matrix. Within this zone, fluid escape structures are a prevalent feature.

Soft sediment deformation features are prevalent throughout the Roseneath and Murteree, varying in thickness from 3-40cm, indicative of a water saturated environment. Rare fluid escape structures are also present. Bioturbation represents a minor feature, which combined with the abundant planar lamination implies oxygen depletion. However, slight increases in the amount of bioturbation up core imply stages of increased oxygenation.

The Epsilon Formation, only present within the Encounter 1 core, is dominated by cross bedded fine to medium grained moderately sorted quartz and mica rich sandstones deposited from tractional currents indicating a higher energy flow regime than that typical for the Roseneath and Murteree. 0.5-15cm thick interbeds of carbonaceous and

sideritic silts are also present within the Epsilon Formation. Based on previous interpretations that this system represents a fluviodeltaic environment, it is likely that these carbonaceous muds and silts represent overbank flood deposits (Gatehouse 1972, Thornton & Hudson 1979, Alexander *et al.* 1998). Bioturbation occurs commonly within organic rich siltstone lithologies of the Epsilon Formation. Siderite, however, is less prevalent then in the Roseneath and Murteree, is not rhythmically interlaminated. Thin coal packages (1cm-15cm) are present within the Epsilon Formation, indicating sub aerial exposure at the time of deposition. These coals are graphitic, indicating that intense thermal maturation has taken place within these sediments.

Grain to grain relations at the micron scale (SEM and microprobe imaging)

Backscattered electron microscope (BSEM) imaging of selected samples within the REM indicates a poorly sorted, texturally and compositionally immature greywacke lithology, dominated by ~40% sub angular quartz grains varying in size from 5 microns up to as large as 1mm (rarely larger than 50µm) (Figure 6, a). Detrital mica (defined as such by its 5-40 µm grain size, distinct mineral boundaries and tabular shape) is the second most abundant mineral phase present (~20%) within the sequence with grains usually found as broken up fragments of less than 10 µm. Many of the mica grains show compositional banding defined by zones of higher magnesium (appearing darker) and iron (lighter) (Figure 6, b). Zinc and lead sulphides, zircons, and Titanium oxides (ilmenite) are present, but only in very minor abundances as accessory phases. Pyrite occurs very rarely, and does not show up in XRD analysis (Appendix B). Feldspars too were not observed in BSEM, or in any of the samples run for XRD. The detrital mineral phases are poorly sorted, and mica often shows alteration to diagenetic clay phases and siderite.
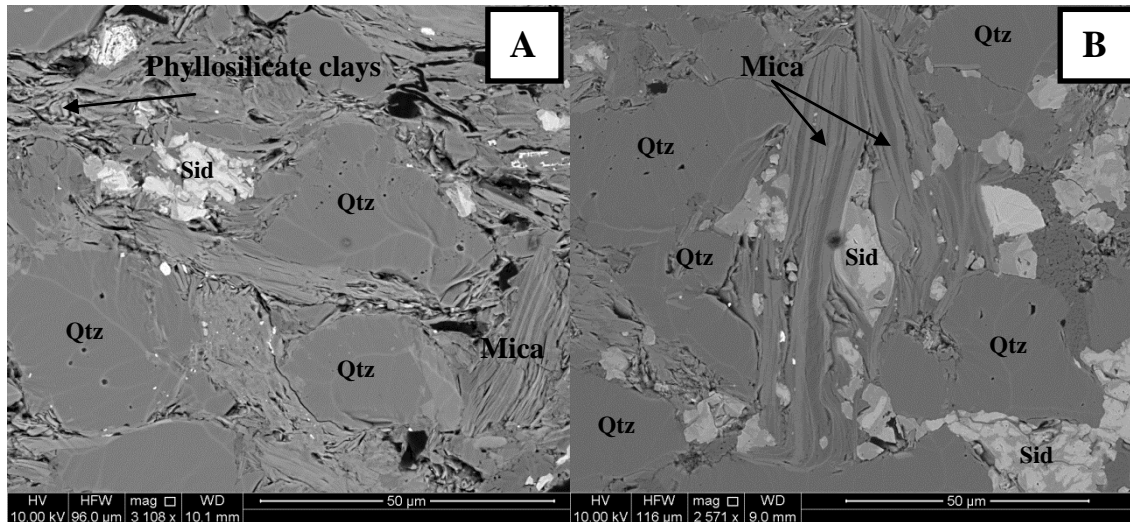
Figure 6: Photomicrographs from the REM indicating the compositionally immature nature of the detrital mineral component. (a) Sub angular to sub rounded quartz (Qtz) grains and detrital mica within a clay matrix dominated largely by illite and broken phyllosilicates. Precipitation of siderite (sid) is also apparent, occurring within the spaces between quartz grains. (b) >50 micron long muscovite grain. EDAX indicates the presence of Fe, Mg, K, Al, Si and O. Darker bands (indicating a lower density) within the mica relate to higher magnesium peaks, while the lighter zones correlate with higher iron peaks. Siderite precipitation within the intergranular pore space is apparent, as well as between mica grains.

The primary clay phase present within the REM is kaolinite, occurring as 10μm size diagenetic books that fill intergranular porosity between quartz and mica grains. Kaolinite is observed commonly as accumulations in >20μm zones which may be indicating replacement of an earlier mineral phase (Figure 8, c). There is conflicting evidence regarding the timing for precipitation of kaolinite within the REM. Kaolinite becomes unstable and undergoes illitisation at temperatures between 120-140 degrees Celsius (Hurst & Kunkle 1985, Lanson *et al.* 2002). However, the burial temperatures based on RockEval data imply mid to late oil window (Vintage Crop 1, %Ro=0.75- 0.95) and dry gas window (Encounter 1, %Ro= 3.60- 3.92) maturities. Therefore, the presence of a stable kaolinite phase within both cores implies a late diagenetic origin. This is supported by BSEM photomicrographs of Epsilon coals from Encounter 1, which show kaolinite books precipitating within coal cleats (Figure 7, a). Such

precipitation could only occur as a later event, after transformation of peat into coal.

Within the Murteree Shale of Vintage Crop 1, at 1958.9m (Ro=0.85) a cement filled

fossil algal cell was observed (Figure 7, b). While diagenetic books indicative of

kaolinite were not observed within this fossil, Energy Dispersive X-ray Analysis

(EDAX) indicated the cements contained only aluminium, silica and oxygen. Clay XRD

indicates the presence of kaolinite, illite, iron-chlorite and mixed illite-smectite within

REM samples. However kaolinite is the only clay mineral of these that would not show

up peaks for iron or potassium in EDAX. For the cell to have survived compaction

under the weight of overlying sediments, it would have required cement precipitation

within its body cavity to have been very early. This implies one of two things: Either a

very early form of kaolinite cement occurred and has remained stable into the oil

window without undergoing illitisation, or the kaolinite cement observed within this cell

is the result of replacement of an earlier mineral phase.

Authigenic illite clays are also apparent in BSEM, indicated by the <1µm crystal size,

growth of aggregated needle-like crystals and EDAX peaks indicating the presence of

potassium, aluminium and oxygen (as well as rare iron peaks). While kaolinite and illite

are responsible for a majority of intergranular pore occlusion within the REM, a

secondary porosity has developed between the growing phyllosilicates which accounts

for the bulk of remaining porosity.
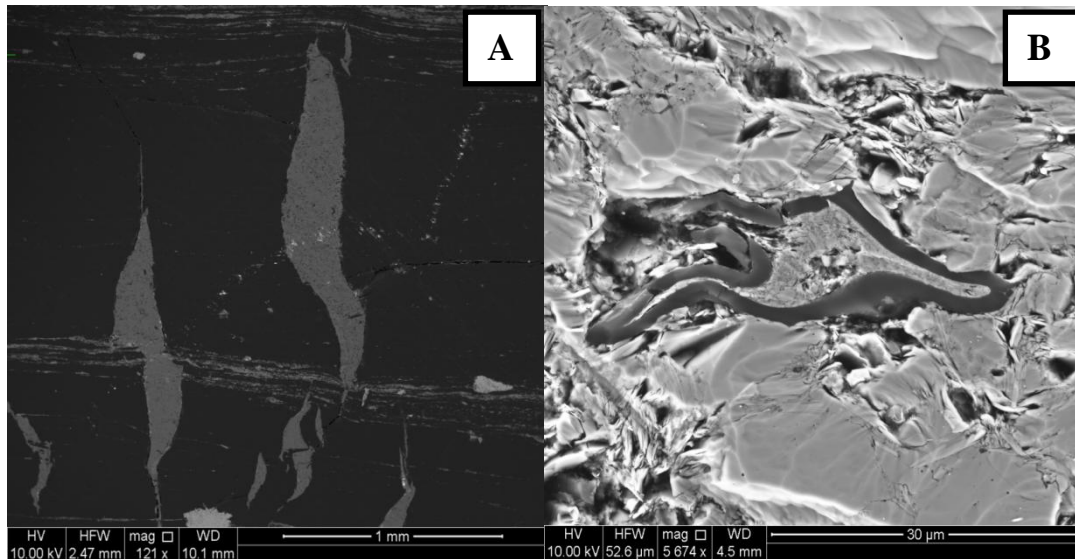
Figure 7: Photomicrographs showing kaolinite cement precipitation (a) Kaolinite cement filling the cleat space within the Encounter 1 Epsilon coal (depth= 3393.5, %Ro= 3.83), indicating a post-coalification diagenetic event. (b) Fossilised algal cell filled with kaolinite cement (based on EDAX peaks for Al, Si and O) from the Murteree Shale, Vintage Crop 1 (depth=1958.9m, %Ro= 0.85).

Bulk powder XRD indicates siderite as the only present carbonate mineral within the REM, existing as an iron rich and magnesium rich phase. Based on XRD and BSEM, siderite is observed within each formation within the REM, however is far less prevalent within the Epsilon Formation. 2 distinct crystal forms are apparent at the micron scale: 2-20μm sized iron rich crystals that exists in the pore space between detrital quartz grains and along permeability pathways (herein referred to as microcrystalline siderite) (Figure 8, b, c), and 20-150μm sized crystals of mixed iron and magnesium composition (herein referred to as sparry siderite) associated with spaces which do not appear to be intergranular pores (Figure 8, d). Sparry siderite is often observed growing around and between detrital mica grains or replacing earlier illite clay phases which now appear depleted in iron and magnesium (Figure 8, f). Based on this observation, it is likely that sparry siderite grew into spaces created by the

breakdown of earlier mineral phases, and that the breakdown of these minerals provided a local source of iron and magnesium. Figure 8e shows siderite precipitation occurring as numerous bladed crystals growing inwardly into available space, which suggests that at least in some cases, the breakdown of earlier phases was completed prior to siderite precipitation. Alternatively, Figure 8e could be representing the dissolution and re-precipitation of an earlier siderite phase at the centre of the crystal.
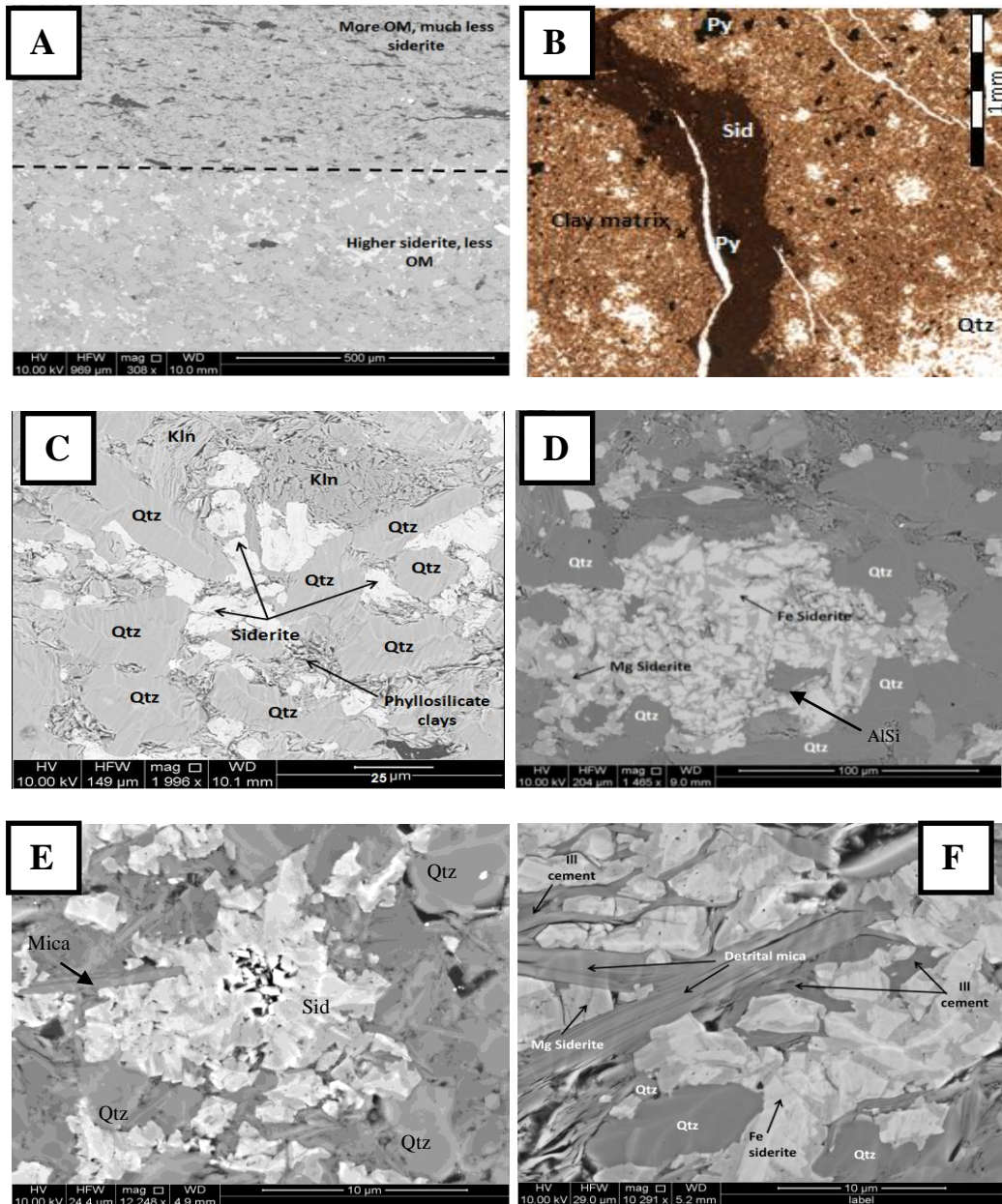
Figure 8: Core photographs and SEM micrographs showing the nature of siderite development within the Roseneath and Murteree Shales. . (a) SEM image of the boundary between a zone dominated by organic matter and one with a much higher siderite abundance (depth= 1958.9m, %Ro=0.85) (b) Petrographic thin section photograph showing siderite (Sid) penetrating into a clay matrix (depth=3554.3). The siderite follows an apparent permeability pathway. Later stage pyrite (Py) precipitation is evident, although pyrite precipitation is uncommon within REM sediments (c) SEM micrograph from the Murteree Shale, Vintage Crop 1 (depth= 1958.9m, %Ro=0.85) indicating microcrystalline siderite precipitation within the intergranular pore space. Phyllosilicate clays are also present within the intergranular pore space. A 30 micron zone of pervasive kaolinite (kln) precipitation is also apparent, which may be representing the replacement of an earlier mineral phase (d) SEM micrograph of sparry siderite, showing complex intergrowth of Fe and Mg dominated phases (depth= 1945.0m, %Ro=0.76). 20 micron pockets of aluminosilicate (AlSi) material, as confirmed by EDAX, within the sparry siderite crystal may be remnants of an ealier mineral phase that is being replaced (e) SEM micrograph of sparry siderite surrounded by a detrital quartz and mica matrix (depth= 1945.0m, %Ro=0.76). Within the centre of the sparry siderite crystal, open space is being filled by inwardly growing, bladed siderite crystals. The presence of this available space indicates either a time lapse between dissolution of an earlier mineral phase and the precipitation of siderite, or that the siderite itself was dissolved and then reprecipitated (f) SEM micrograph showing the breakdown of detrital mica, as well as the precipitation of Mg and Fe siderite (sid) and illite (Ill) cement ((depth= 1945.4m, %Ro=0.78). Siderite appears to be growing between a fabric within the mica grain, forcing it to be split open. Further siderite grains are observed precipitating surrounded by illlite, which is being displaced by the siderite growth. The spatial associations suggests siderite is forming from the breakdown of the mica and illite.

The combination of the pore-filling nature of the siderite and the complete lack of recognisable allochems implies a diagenetic origin for siderite precipitation. Oxygen isotopic evidence also indicates a diagenetic origin for siderite, assuming that O^{18} fractionation is the result of temperature. Isotope excursions within Vintage Crop 1 samples vary between -8.29‰ and +3.94‰ for carbon, and -16.45‰ and -13.96‰ for oxygen. The heavily oxygen depleted values, the $R^2=0.95$ covariance between carbon and oxygen (Figure 9), and the apparent lack of a stratigraphic or lithological control on isotope variability suggests a diagenetic role exists in the precipitation of siderite, with isotopic variations the result of mixing between two end members. Siderite within the REM has a dominantly iron rich composition (appear white in BSEM), however phases of magnesium rich siderite (darker grey) precipitation is present, particularly associated with sparry siderite, and electron microprobe imaging also shows the presence of calcium and manganese (Figure 10, a-e). Magnesium and iron phases show complex zonation, however Mg-rich siderite is often observed forming at crystal edges, suggesting that it is a later developed phase. Assuming that the different siderite phases have not co-precipitated, it is likely that observed isotopic variations are the result of mixing between Fe and Mg phases that have precipitated with differing fluid water chemistries.
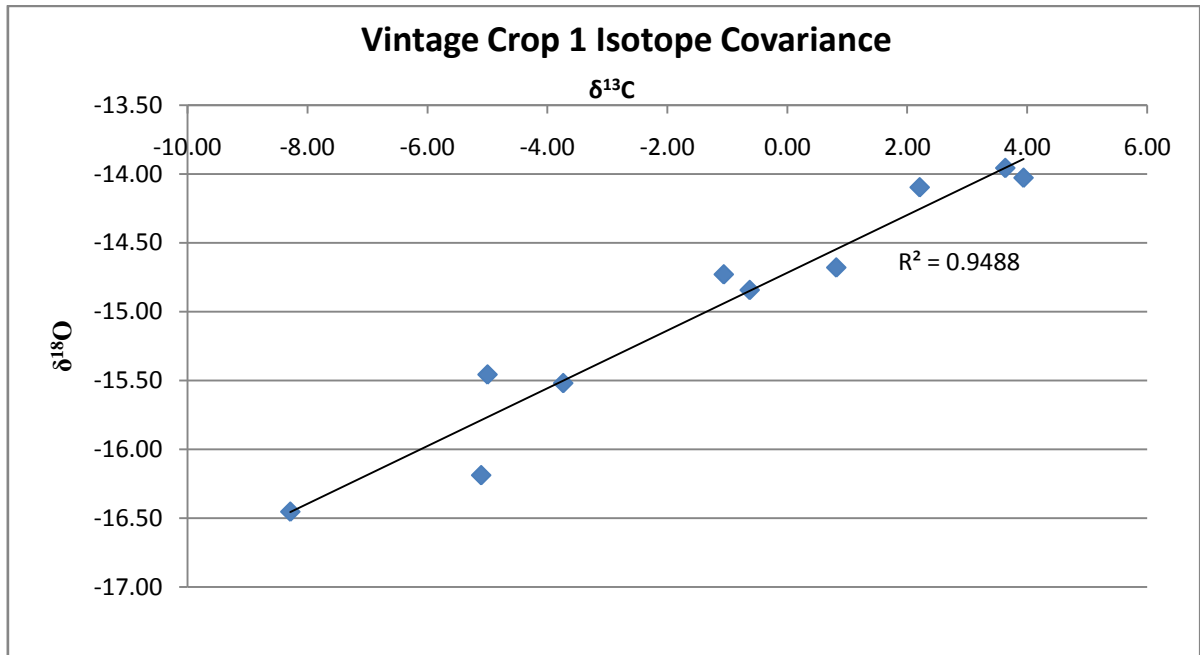
Figure 9: Cross plot showing the $R^2 = 0.95$ covariance of carbon 13(δ13C) and oxygen 18(δ18O). Variations in carbon and oxygen isotope values are likely the result of mixing between two end member phases. Based on BSEM observations that Fe and Mg phases are present, it is likely these represent the two end member phases
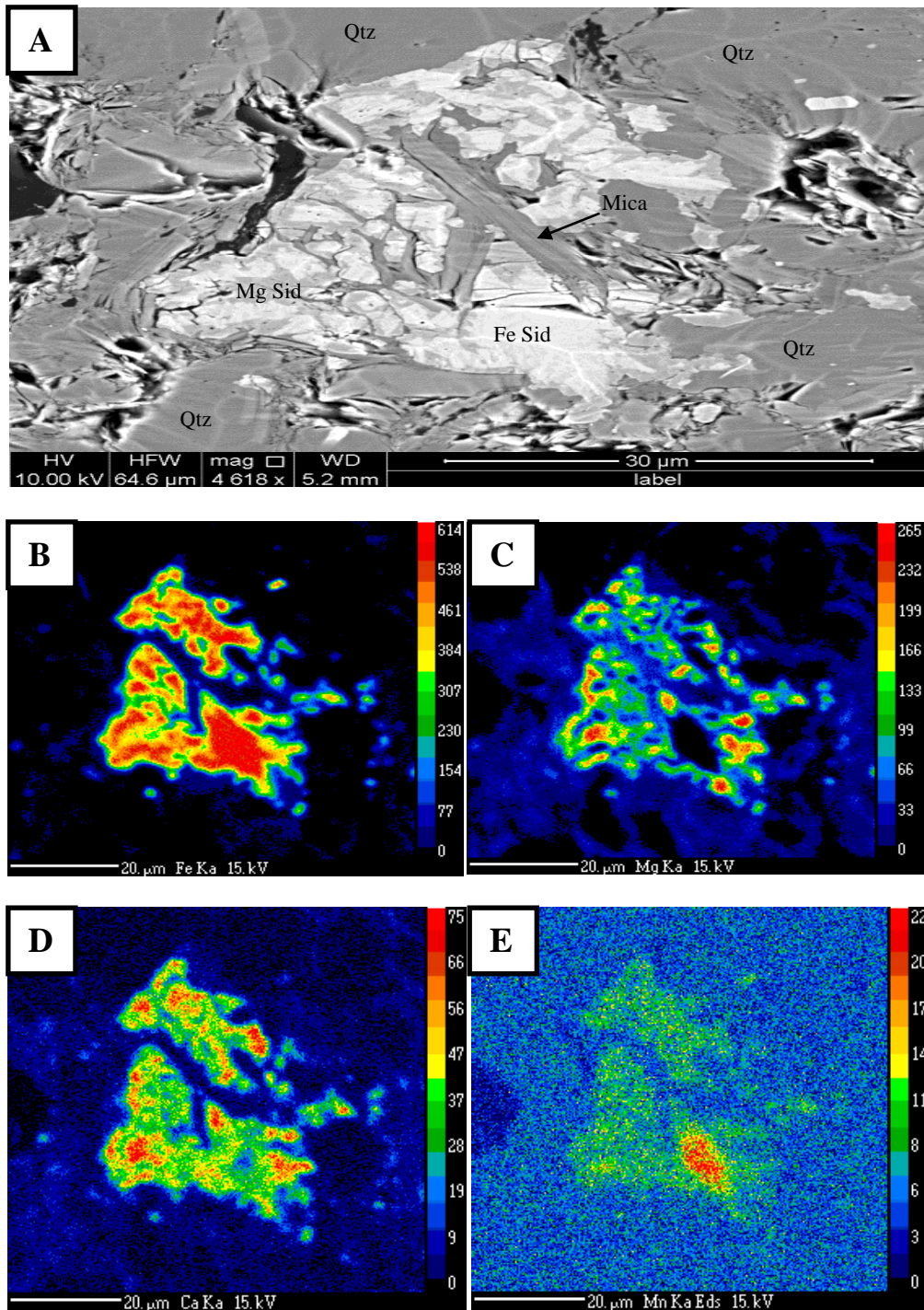
Figure 10: SEM and microprobe photomicrographs of a sparry siderite crystal from the Murteree Shale of Vintage Crop 1 (depth= 1945.4m, %Ro=0.78). (a) SEM image showing a the breakdown of a detrital mica grain, the development of illite cements and the precipitation of Mg and Fe siderite from the breakdown of mica and illite. Note that Mg siderite appears most prevalent at the edges of the sparry siderite (b) Electron microprobe image showing the distribution of iron (Fe) within a single siderite grain. Iron appears to be the dominant phase present, as indicated by the spatial distribution. (c) Electron microprobe image showing the distribution of Magnesium (Mg) within the same siderite grain. Magnesium appears to be a less dominant phase than iron, however isolated regions of high peak intensity are present (d) Electron microprobe image showing the distribution of Calcium (Ca). A spatial relationship exists between high peak intensities for Mg and Ca (e) Electron microprobe image showing the distribution of Manganese (Mn). A spatial relationship exists between high peak intensities for Mn and Fe

Using BSEM and microprobe imaging, grain size variations were observed in 0.5-1mm thick laminations taken from rhythmically laminated zones within the Roseneath Shale of Vintage Crop 1 (depth= 1958.9m). Laminae with quartz and mica grain sizes of 30-40μm and larger pore spaces show an increased abundance of siderite (Figure 11, c, e). Conversely, in laminations with a smaller overall grain size (~5μm) and smaller pores, siderite is less abundant (Figure 11, c, e). Furthermore, pore residing organic matter is observed where siderite is not present, principally within laminations with a grain size <5μm, and siderite is more abundant when organic matter is not present (in the laminations with 30-40μm sized grains) (Figure 11, c, d, e). Observed millimetre interlaminations of organic rich and siderite altered siltstone at the core scale appear to be reflecting subtle variations in grain size as a result of deposition of interlaminated silts and fine silt to clay sized sediments. This is also reflected within the geochemical signature of Roseneath and Epsilon samples, with lower TOC values in samples more pervasively altered by siderite (see section on geochemistry below). Furthermore, the observation that organic matter and siderite are not observed coexisting within the intergranular pore space implies a difference in the timing of organic matter emplacement and siderite precipitation.
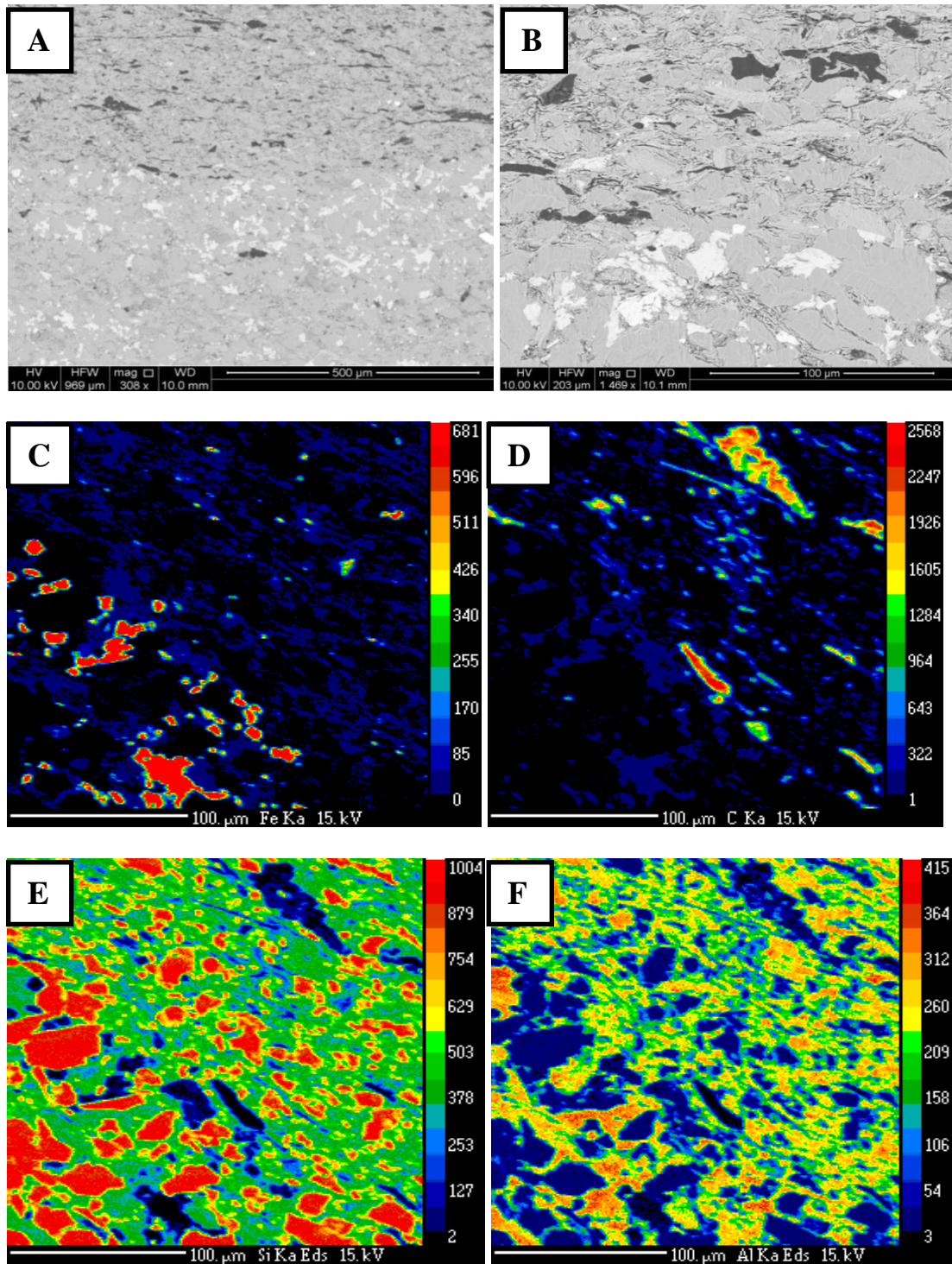
Figure 11: SEM and microprobe photomicrographs for a boundary between a sideritic and carbonaceous band from the Murteree Shale, Vintage Crop 1 (depth= 1958.9m, %Ro=0.85). (a) SEM image of the boundary between a zone dominated by organic matter and one with a much higher siderite abundance (b) Zoomed in image for figure a, in the proximity of the zone that was selected for microprobe analysis (c) Electron microprobe image of iron (Fe) content, showing a sharp boundary between where siderite can and cannot develop (d) Electron microprobe image of carbon (C) content, showing the distribution of organic carbon is limited to the upper layer (e) Electron microprobe image of silicon (Si) content. Note the discrepancy in grain size between those of the lower, more siderite dominated band and the upper carbonaceous band. (f) Electron microprobe image of aluminium (Al) content, showing that aluminium occurs pervasively across both bands. It is likely that these high aluminium values are derived from the presence of illite and kaolinite.

Iron mapping was conducted on a 2cm long thin section of Roseneath Shale laminae from Encounter 1 (3270m) using the X ray fluorescence line at the Australian Synchrotron (Figure 12). At a resolution of 4 microns, figure 12 shows rhythmic 0.5-5mm bands of siderite, occurring at intervals between 1 and 1.5mm. These bands show pervasive iron concentrations at the base and grade upwards. Based the microprobe images for Vintage Crop 1 shown in figure 10, a-f, it is likely that these siderite dominated bands comprise coarser grained minerals and greater pore space, and that zones where siderite are less pervasive are finer grained, have less pore space and are dominated by clays. This suggests a cyclic, deposition driven mechanism on where siderite can later develop controlled by grain size and available porosity rather than depositional chemistry.
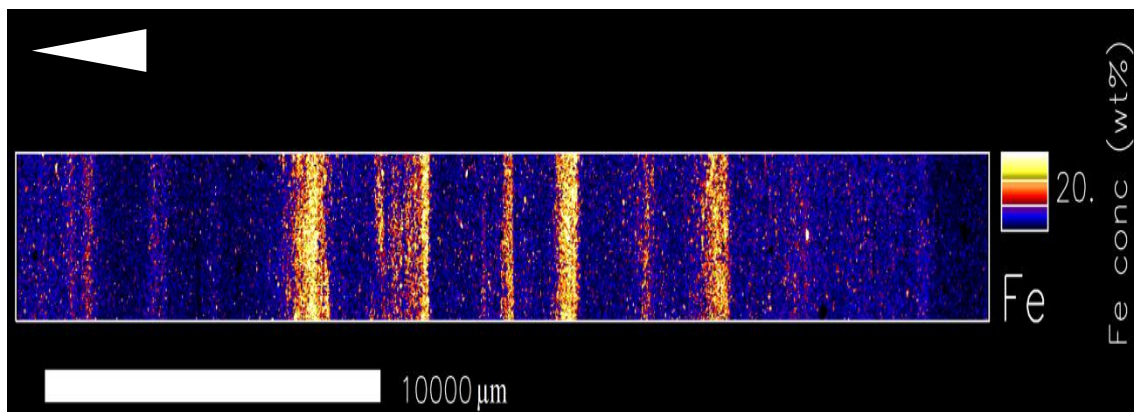
Figure 12: Iron map indicating the presence of 0.5-5mm rhythmic laminations of siderite within the Roseneath Shale of Encounter 1 (depth= 3270m). Colour intensity represents the weight percentage of iron present. Sideritic laminations occur approximately every 1-1.5mm, and are particularly prevalent within a central 1.5 cm zone at the centre of the image. Each siderite lamination has a pervasive base and grades upwards. The white arrow at the top left of the image indicates direction of grading.

Organic matter

Based on BSEM of selected samples within the REM, organic matter varies in size from less than 1μm up to over 200μm, and is present almost entirely as dispersed organic matter. No pores are observed within any of the organic matter samples, despite oil window (Vintage Crop 1) and dry gas window (Encounter 1) maturities. As highlighted earlier, organic matter is more commonly associated with laminations dominated by finer minerals, where there is a smaller pore space and lower siderite abundance (Figure 13, a). 3 main organic matter forms were observed under BSEM: pore residing, detrital plant material and accumulated particulate (described below). These 3 forms of OM were found commonly within the Roseneath, Epsilon and Murteree formations, which may imply a similar OM source for all 3 formations. The major variation between the formations is in the abundance of organic matter, with the Epsilon Formation containing considerably more (organic geochemistry indicating TOCs as high as 8% in Epsilon Shales). This increase in organic carbon coincides with a decreased abundance in siderite within the Epsilon Formation.

The dominant form of organic matter observed within REM samples are 20-50μm sized particles with tabular or spherical shapes and clear defined boundaries (Figure 13, a, b, c). In many samples, the spherical organic matter has been compressed to form elongate flattened shapes often with cement filled centres (Figure 13, d). Based on the regular, defined shapes, this material is interpreted to be fragments of plant detritus and spores. This is supported by organic petrography conducted by Weatherford Laboratories (2012) from Vintage Crop 1 on Roseneath and Murteree shale core samples, which indicates inertinite and vitrinite to be the most abundant maceral types (with a minor

algal signature), based on shape, reflectance and fluorescence using oil immersion optical microscopy. Smyth (1985) also highlighted an abundance of inertinite and vitrinite, although this study was conducted on REM chip samples from the Patchawarra Trough. Less commonly, >200μm grains of tabular shaped OM, which are an order of magnitude larger than surrounding OM material, are present (Figure 14, e). Within these tabular particles, interconnected 10-50μm sized zones exist which are filled with clays. It is unclear from the image whether this is the result of localised breakdown and replacement of organics, or if clays are simply forming within natural spaces within the grain. While these large tabular OM particles could be interpreted to be larger fragments of plant detritus, it is also possible that these are a detrital coal or shale fragments.
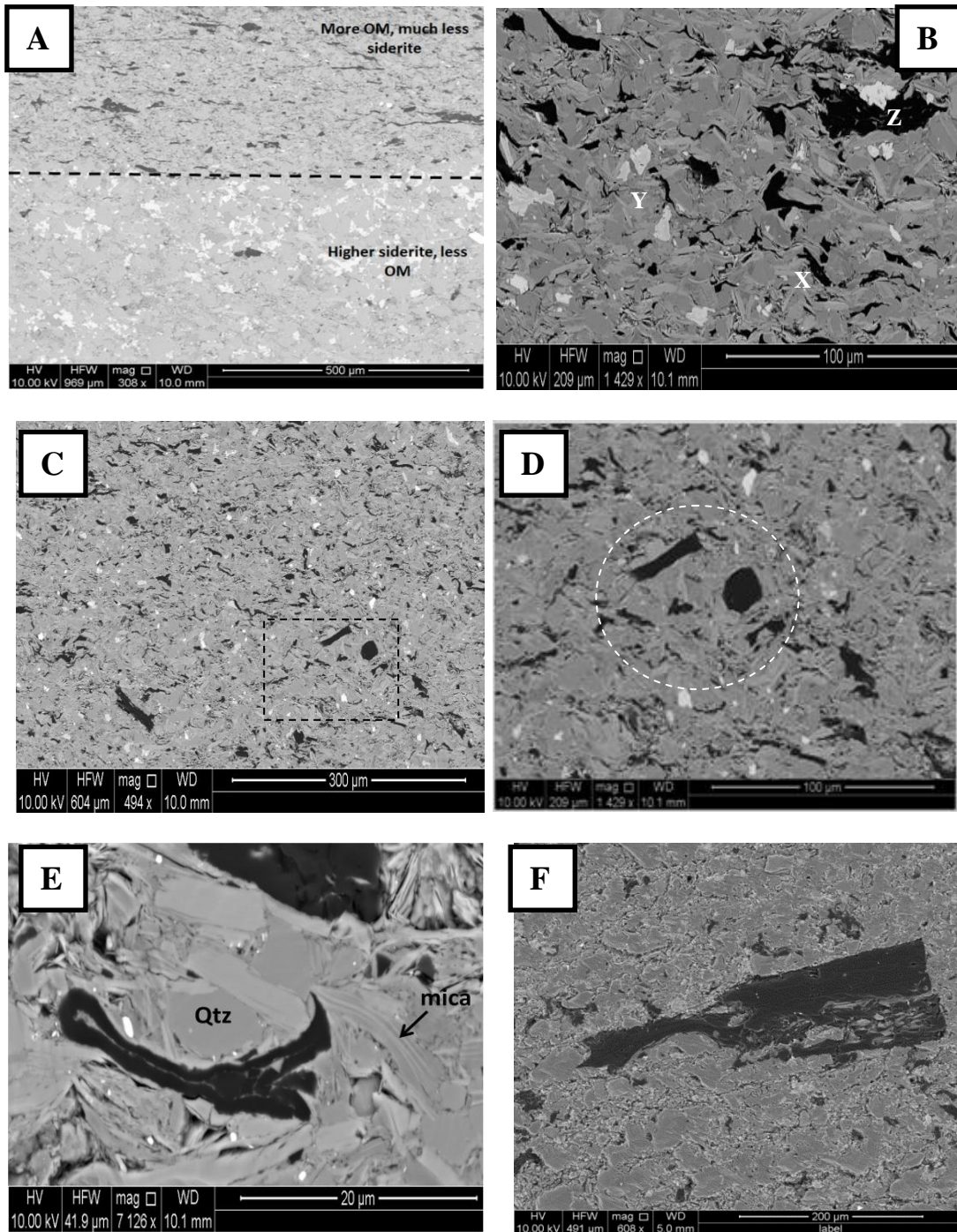
Figure 13: SEM micrographs showing common organic matter types present within the REM. (a) Photomicrograph from the Murteree Shale, Vintage Crop 1(depth=1958.9m, %Ro=.85, TOC=2.0) indicating the interlaminated nature of organic carbon and siderite development. Note in particular that organic carbon and siderite do not coexist (b) Photomicrograph from the Epsilon Formation of Encounter 1 (depth=3395.8m, %Ro=3.83, TOC=4.5). Note the presence of tabular, 20 micron sized plant detritus (x), pore residing organic matter (y), and aggregated organic matter (z) forms within a single image (c) Photomicrograph from the Epsilon Formation of Encounter 1 (depth=3395.8m, %Ro=3.83, TOC=4.5) showing the well-defined OM shapes that have been described as detrital plant matter (d) Zoomed in image of figure c, with the well defined OM shapes are circled in white (e) Photomicrograph from the Murteree Formation, Vintage Crop 1 (depth=1945.4, %Ro=0.78, TOC=3.3) of an elongate, deformed organic matter particle with a cement centre, interpreted to be a plant spore that has been compressed by surrounding minerals during compaction. (f) Photomicrograph of a >200 micron sized fragment of organic matter from the Murteree Shale, Vintage Crop 1 (depth=1945.0, %Ro=0.76, TOC=3.8). Note the well-defined shaped and the significantly greater size than the surrounding material.

Another dominant form of organic matter observed within selected REM samples is less than 20μm, resides predominantly between mineral grains and has a shape defined by surrounding mineral grain contacts (Figure 14, a). While potential exists that compressive stresses exerted on deposited organic matter by surrounding mineral grains during burial and compaction have resulted in deformation of OM, it is equally likely that this organic matter represents a migrated hydrocarbon phase. This is particularly true of Figure 14b, as the organic matter is observed as a mineral coating feature.

50μm sized ellipsoidal agglomerations of organic matter, illitic clays and <10μm detrital quartz and mica grains are also observed within REM samples (Figure 14, b). The organic matter has clearly defined borders not defined by surrounding mineral grain contacts, and in a number of examples contains internal chambers within which the bulk of clay and other detritus are observed (Figure 14, c, d). In other cases, the clays are present as elongate, undulating lenses (Figure 14, b). Due to the size, shape and mixing of clays and organic matter, these organic-clay associates have been interpreted as faecal pellets, with the chambered areas represented in figures 14 c and d the fossil remnants of chambered organisms such as foraminifera which are become filled with sediments.
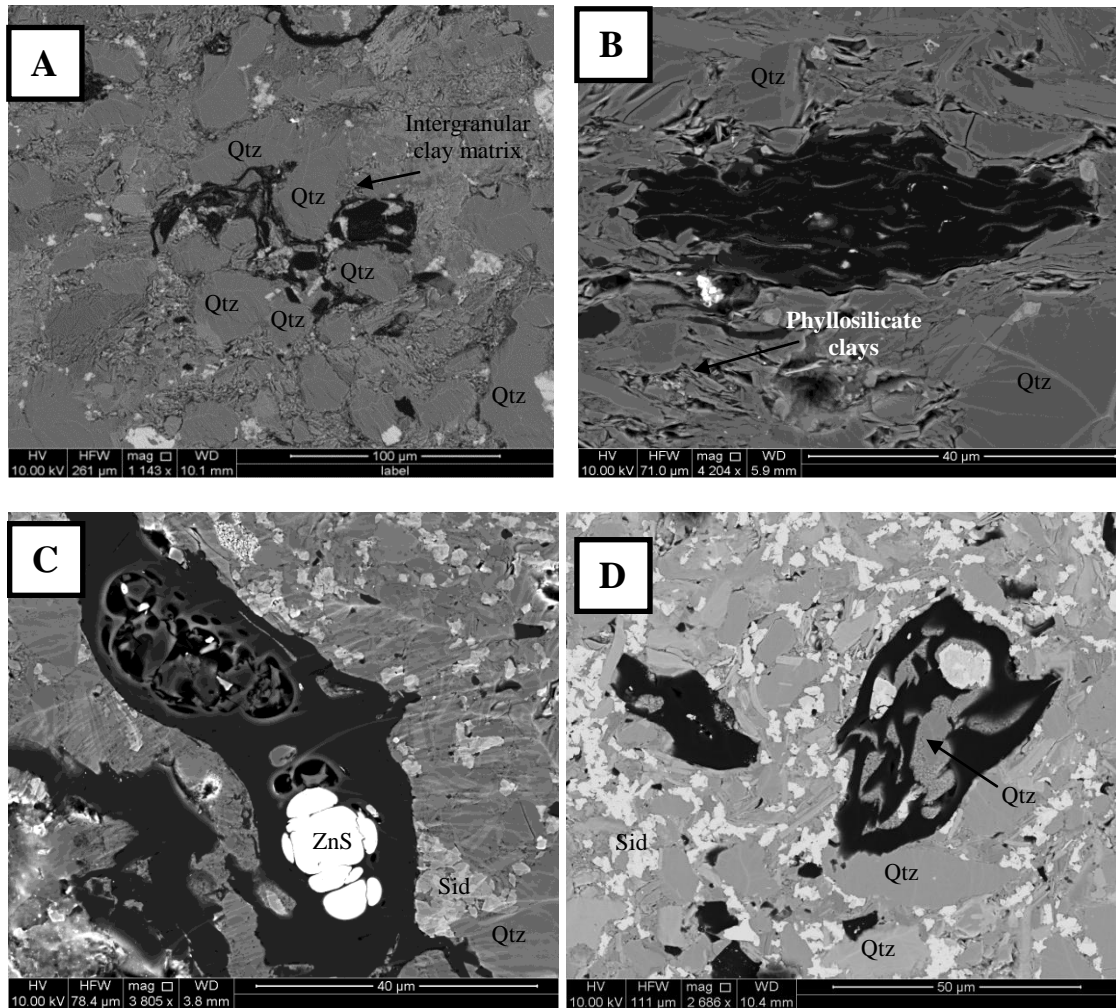
Figure 14: SEM micrographs showing other organic matter types present within the REM.

(a) Photomicrograph from the Murteree Shale, Vintage Crop 1 1 (depth=1945.0m, %Ro=0.76, TOC=3.8) showing organic matter residing within the pore space between a number of 10-30 micron quartz grains. Note the grain coating relationship with the quartz grains, suggesting that this organic matter type is present as a result of migration. Intergranular phyllosillicate clays are also present (b) Photomicrograph of a 50 micron agglomerated particule of organic matter from the Murteree Shale, Vintage Crop 1 (depth=1945.4m, %Ro=0.78, TOC=3.4). Note that the 50 micron sized organic matter contains elongate isolated bodies of clay. (c) Photomicrograph from the Murteree Shale, Vintage Crop 1 (depth=1945.0m, %Ro=0.76, TOC=3.8) showing a 100 micron long particle of organic matter, which contain chambered spaces. EDaX analysis shows that bright minerals present within these spaces are Zn sulphides (ZnS). Mineralogy surrounding the OM particles is comprised dominantly of 10- >40 micron sized grains of sub angular quartz. Siderite (grain size between 1-20 microns) is present between grains of quartz, and is also found growing against the OM particle. (d) Photomicrograph from the Murteree Shale, Vintage Crop 1 (depth=1945.0m, %Ro=0.76, TOC=3.8) showing 50 micron sized OM particles that contain chambered spaces between 1 and 10 microns in size that have been filled by siderite and illite cements, as well as rare detrital 10 micron sized quartz grains. Outside of the OM, microcrystalline siderite exists within the intergranular pore space between 10-50 micron sized quartz grains and 10-20 micron sized mica grains along with phyllosilicate clays.

Phase relationships for organic matter and diagenetic cements

As highlighted in figures 11 and 13a, there is a difference in timing between emplacement of pore residing organic matter and the precipitation of siderite. If the pore residing organic matter indeed reflects a migrated hydrocarbon component, understanding the timing of diagenetic clay and carbonate emplacement is pivotal in determining how migration has occurred.

Figure 15, a, a zoomed in micrograph of a chambered zone within a faecal pellet described in figure 14, d indicates illite precipitation preceded siderite development. The matrix within this organic walled chamber is dominated by micron sized clays interpreted to be illite due to EDAX returning peaks for potassium, aluminium, silicon and oxygen. A mix of illite types is represented in both needle-like crystals and rounded grains. The <1μm size and the presence of needle like crystals implies a diagenetic origin for some of this illite, however there is likely a detrital component present also. The siderite inclusion is occurring as a result of replacement of the earlier illite phase, evident in the presence illite inclusions within the siderite crystal. This illite replacement was noted earlier based on observations from figure 8f. Zonation between iron and magnesium siderite is apparent, suggesting 3 separate phases of development, the first and last of which appear to be iron dominated. This contradicts earlier observed siderite phase relationships, which indicate the magnesium rich phase to be the latest. The Siderite crystal also appears to be breaking down portions of the organic matter.

Siderite precipitating as a result of organic matter and illite clay breakdown is further evidenced in figures 15 c and d. A 50μm sized sparry siderite crystal, which comprises a

number of smaller (5-20μm) crystals, is present growing within a matrix of organic matter and illite. Fe (light grey) and Mg (dark grey) phases are both present. The Mg phase is most prevalent at crystal boundaries in proximity of organic matter and illite. 2 crystal boundary styles are observed: bladed edged crystal development and curved boundary crystal development (the latter being the more common feature observed).

Organic matter is present between the siderite crystals, predominantly as lobate features interlaminated with needle-likediagenetic illite. The orientation of organic matter and illite interlaminations follow the contours of siderite growth, suggesting siderite is causing fabric displacement. This is also observed in figure 12b. Sub-micron inclusions of organic matter are present within siderite crystals. OM is also present as accumulations within the intergranular pore space between 10-50 micron sized quartz grains surrounding the sparry siderite crystal (Figure 15, c). This may be the result of local migration of organic matter as a result of displacement by the growing sparry siderite, which would require oil window temperatures.

As was highlighted earlier, the presence of stable kaolinite phase within Vintage Crop 1 and Encounter 1 cores implies kaolinite was a later diagenetic event, which was supported by observational evidence of kaolinite precipitating within Epsilon coal cleats (Figure 7, a). This is likely post illlite and siderite precipitation, as a result of later diagenetic fluids interacting with and dissolving mica and illite, evident through the present of >20 micron accumulations of kaolinite books in zones too large to be intergranular pore space. The timing of iron chlorite precipitation is less clear, as

observations of this clay phase were not noted using BSEM techniques, but through

clay XRD.
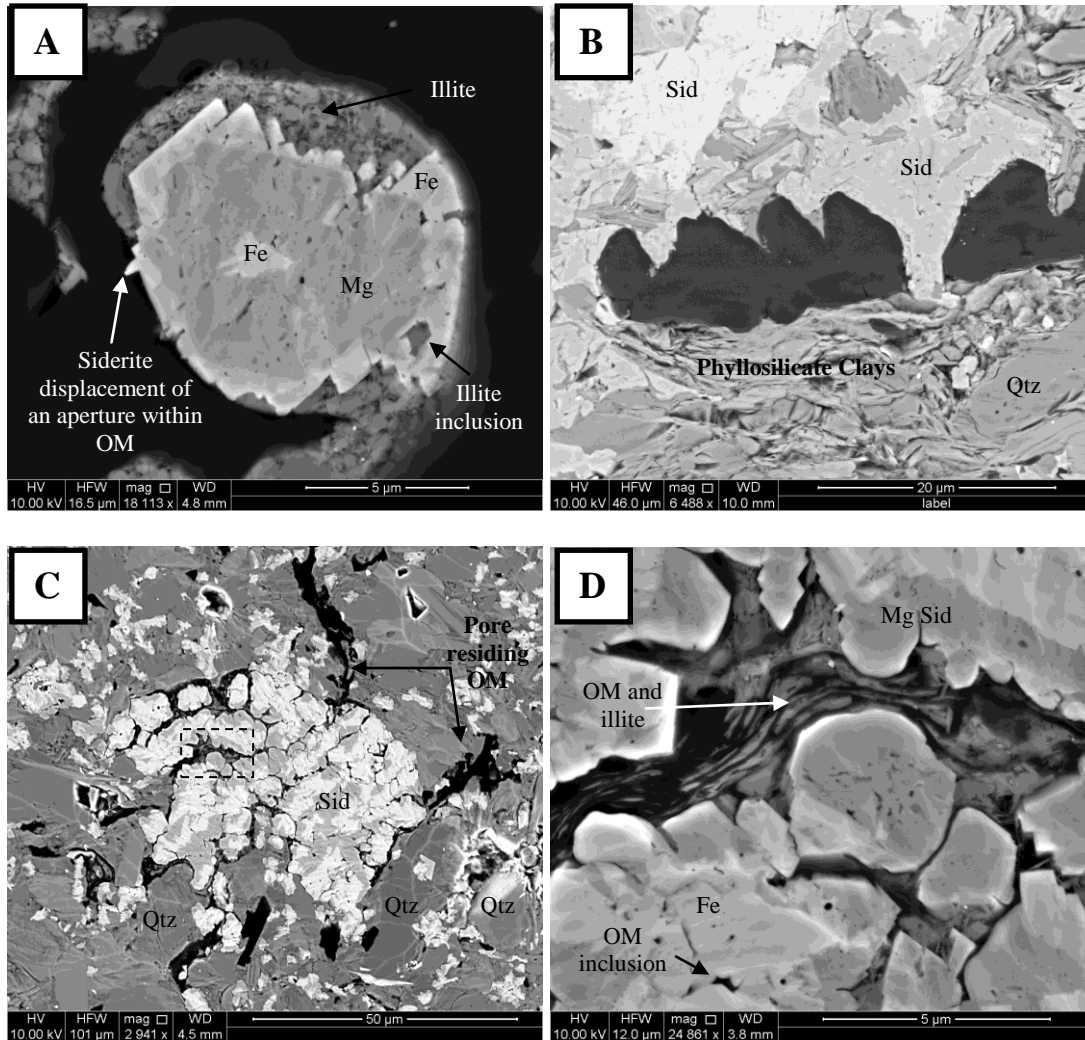
Figure 15: Phase relationships between organic matter, illite clays and siderite. (a) Zoomed in photomicrograph from the Murteree Shale, Vintage Crop 1 (depth=1945.0m, %Ro=0.76, TOC=3.8) of a illite filled chambered zone within a faecal pellet. Siderite is forming from replacement of illite, inferred from the presence of illite inclusions within the siderite crystal. The siderite growth is also displacing small zones of the organic matter. (b) Photomicrograph from the Roseneath Shale, Vintage Crop 1 (depth=1842.1m, %Ro= 0.83, TOC=1.0) showing the effect fabric displacive growth of siderite on organic matter particles. The OM particle is become disaggregated and deformed as a result of siderite growth. (c) Photomicrograph from the Murteree Shale, Vintage Crop 1 (depth=1945.0m, %Ro=0.76, TOC=3.8) showing replacement of organics and illite by sparry siderite. Sparry siderite comprises several smaller crystals surrounded by organics and illite. The progressive growth of these siderite crystals has resulted in deformation of the organic matter and illite. Organic matter is also present in the intergranular pore space between quartz grains not associated with the growing sparry siderite, which could represent a migrated hydrocarbon phase. (d) Zoomed in photomicrograph from figure c, highlighting the deformation of organic matter and illite by siderite growth. Note the presence of both bladed and curved crystal boundaries for siderite, as well as the increased proportion of Mg rich siderite in close proximity to the illite and organics.

Geochemistry

Across the REM section of Vintage Crop 1 and Encounter 1 cores, TOC varies between

0.9% and 82.0% (Table 2). The Epsilon Formation shows the highest average TOC, due

largely to the presence of coals which skew the data for this formation. However, TOCs

from carbonaceous siltstone samples within the Epsilon Formation vary between 1.3

and 8.4%, a higher abundance than that observed within the Roseneath and Murteree

Shales.

Table 3: Summary of TOC variations across the REM formations for Vintage Crop 1 and Encounter 1 cores. Organic matter varies between 0.9 and 82%.

	Vintage Crop- 1		Encounter-1		
TOC (%)	**Roseneath Shale**	**Murteree Shale**	**Roseneath Shale**	**Epsilon Formation**	**Murteree Shale**
Mean	2.59	2.74	3.09	10.38	2.23
Std Dev	0.63	0.55	0.59	22.63	0.54
Variance	0.39	0.31	0.35	512.03	0.29
Range	2.65	2.52	2.21	80.69	3.08
Minimum	1.61	1.69	1.87	1.27	0.88
Maximum	4.26	4.22	4.09	81.96	3.96
Count	32	32	15	12	33

For samples measured for TOC every 5mm, at least 2 separate cycles, occurring at

different scales become apparent (Figure 12). Centimetre scale cycles are associated

with variations on the order of 0.25-0.5% TOC. BSEM imaging indicates variations

between TOC rich and poor laminations to be occurring at a mm scale, which suggests

that each high resolution measurement taken is still an amalgamation of several smaller

cycles. Another potential cycle appears to be occurring every 12cm, associated with

variations between 2.1 and 3.8% TOC. Given the sudden shifts in TOC, it is likely that

this may represent a significant event. However, as high resolution sampling was only conducted on a 15cm interval, the second half of this larger cycle was not obtained to show a consistent pattern. BSEM and microprobe imagery has shown variations in organic matter to track grain size trends at the lamination scale, with higher proportions of organic matter associated with the finer grain size fraction. It is therefore likely that these cycles in TOC are tracking grain size variations relating to differing proportions of depositional units. Increased TOC values likely correlate with a greater proportion of fine depositional units, and low TOC with the coarser siltstone fraction (likely with higher siderite abundance). However, without BSEM on these samples there is no way to be certain.
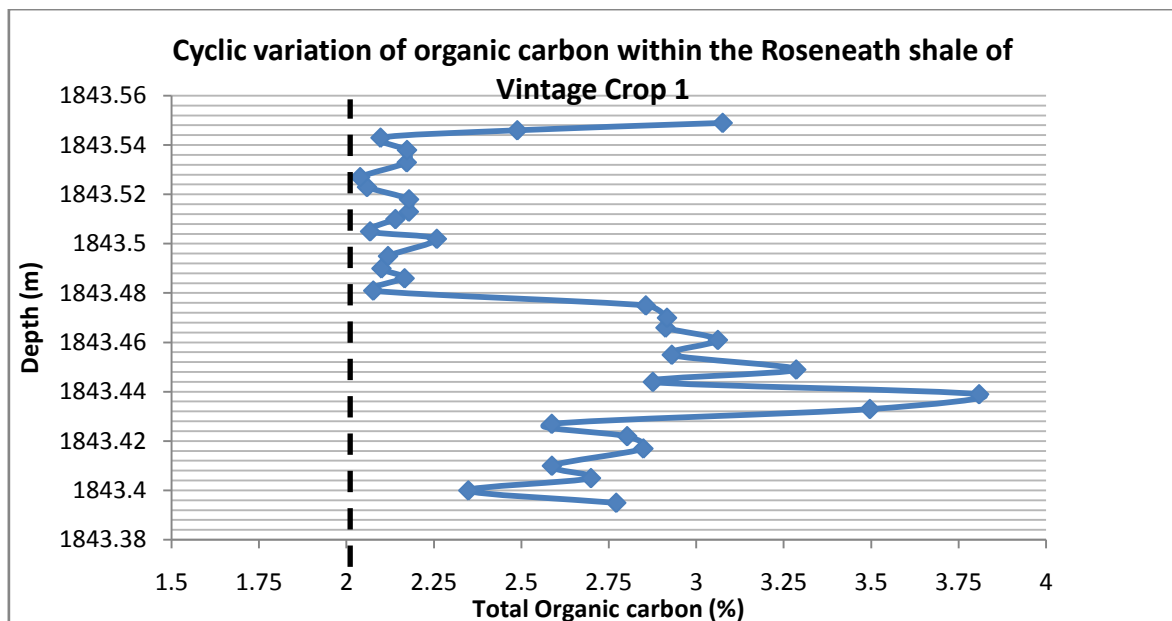
Figure 16: High resolution total organic carbon (TOC) sampling for a 15cm interval of the Roseneath Shale in Vintage Crop 1, showing the geochemical variations present at the minute scale. 2 different cycles of organic matter variation are apparent: one at the sub centimetre scale, associated with minor perturbations and a larger 15cm scale variation in organic carbon which is associated with more pronounced fluxes in organic carbon content. No sample within this high resolution interval fell below what might be considered a potential source rock (2% TOC).

ORGANIC MATTER TYPES WITHIN THE REM

Despite samples from Encounter 1 plotting in the dry gas window and Vintage Crop 1 samples plotting within the oil window (Figure 13, a), both record an organic matter type with low hydrocarbon generating ability when plotted on Van Krevelen diagrams (Figure 13, a, b). Encounter 1 data plots consistently as type IV (inert) organic matter, reflecting its high thermal maturity. Vintage Crop 1 samples plot as type III (gas prone) and type IV, with only a few samples plotting as borderline mixed type II-III (oil prone-gas prone). Rock Eval indicates the free gas (S1) component from organics within the REM for Vintage Crop1 varies between 0.09 and 0.49mgHC/gOC, and between 0.05 and 0.58mgHC/gOC for Encounter 1. Generative potential (S2) from carbonaceous silts varies between 0.3 and 3.0mgHC/gOC, and between 0.1 and 0.51mgHC/gOC for Encounter 1. Coal from the Epsilon Formation from Encounter 1 showed an S2 of 4.42, indicating a significantly greater generative potential exists in REM coals compared with carbonaceous silts and muds.

1
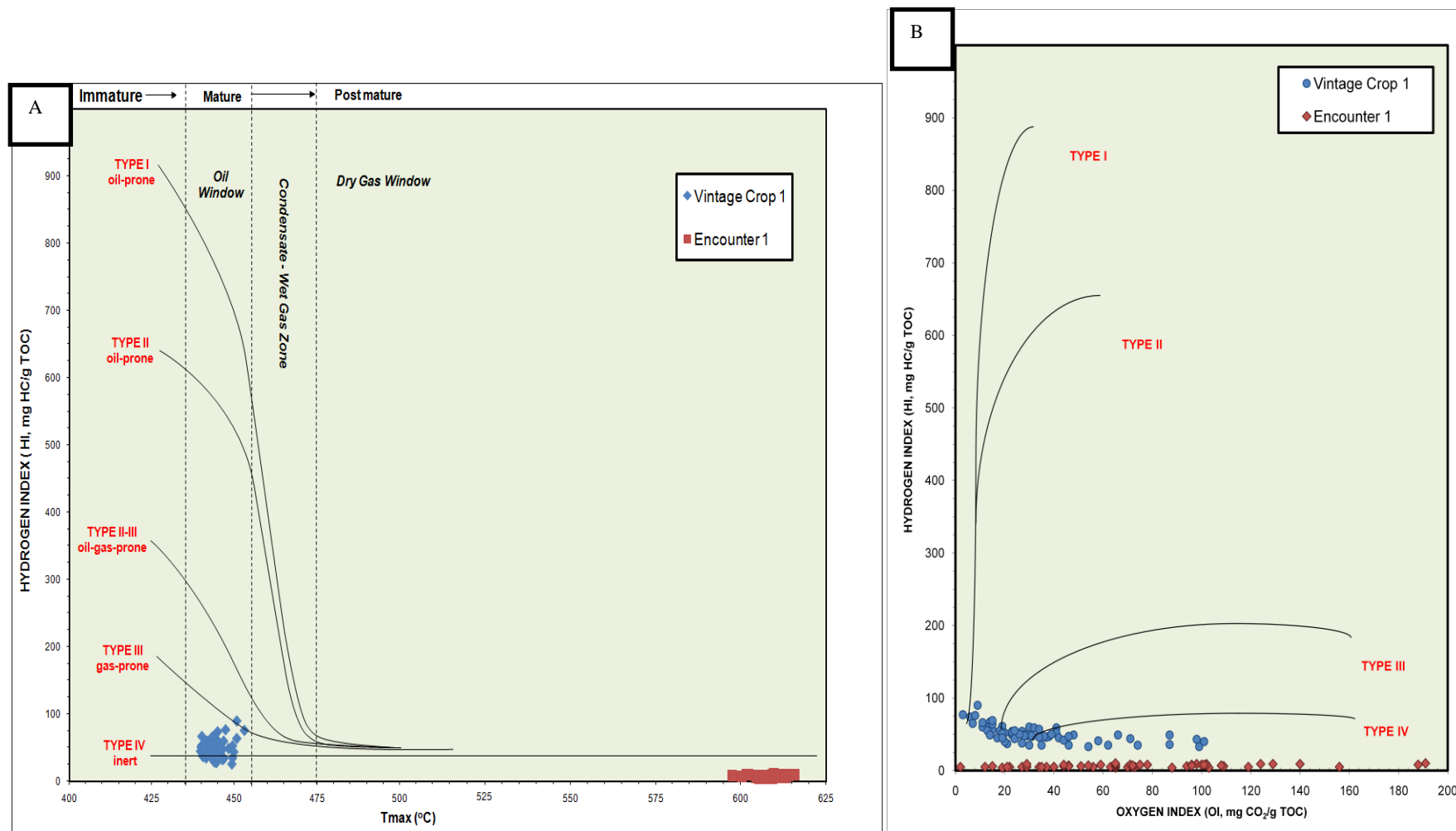
Figure 17: Van Krevelen Diagrams for Vintage Crop 1 (blue) and Encounter 1 (red) samples. (a) Plot of Tmax against hydrogen index, showing that while Vintage Crop 1 is within the oil window, its hydrocarbon generating potential is minimal. (b) Plot of Oxygen Index against hydrogen Index, again highlighting the low hydrocarbon generating potential of Encounter 1 and Vintage Crop 1 organic matter. The majority of data points plot as gas prone to inert.

SURFACE AREA ANALYSIS

Within the Roseneath and Murteree shales, there is no relationship between siderite (FeCO3) corrected mineral surface area and FeCO3 corrected TOC (Figure 18a, c; Figure 16, 17). However, there is a relationship between TOC and MSA in the Epsilon Formation (Figure 15 b; 16 a). The high MSA values within the Epsilon Formation are related to coals and overbank deposited carbonaceous shales, and do not appear to reflect the surface area of minerals. The highest MSA value ($428.48m^2/g$) corresponds with an 88% TOC coal. BSEM comparisons of organic matter from the Epsilon Formation carbonaceous siltstone samples with those of the Roseneath and Murteree do not show a difference in the type of organic matter, and while XRD and BSEM indicates the presence of abundant illite, these are dominantly detrital and not evidently associated with EDAX carbon peaks. However, there is a substantial difference in the abundance of organic matter (1-8% in Epsilon shales opposed to 0.9-4% in the Roseneath and Murteree Shales), which suggests that organic matter abundance has a pronounced impact on the TOC-MSA relationship, even when no apparent clay preservational effect exists.

Samples treated with sodium hypochlorite to remove organic matter consistently showed lower surface area values than those that were untreated (Figure 20, a, b). Difference in MSA varied between +1% and -49%, with an average of 20% reduction in MSA, associated with TOC reductions between 56 and 81%. The difference in TOC after sodium hypochlorite treatment accounts for 72.4% of variation in MSA difference after treatment (Figure 21).
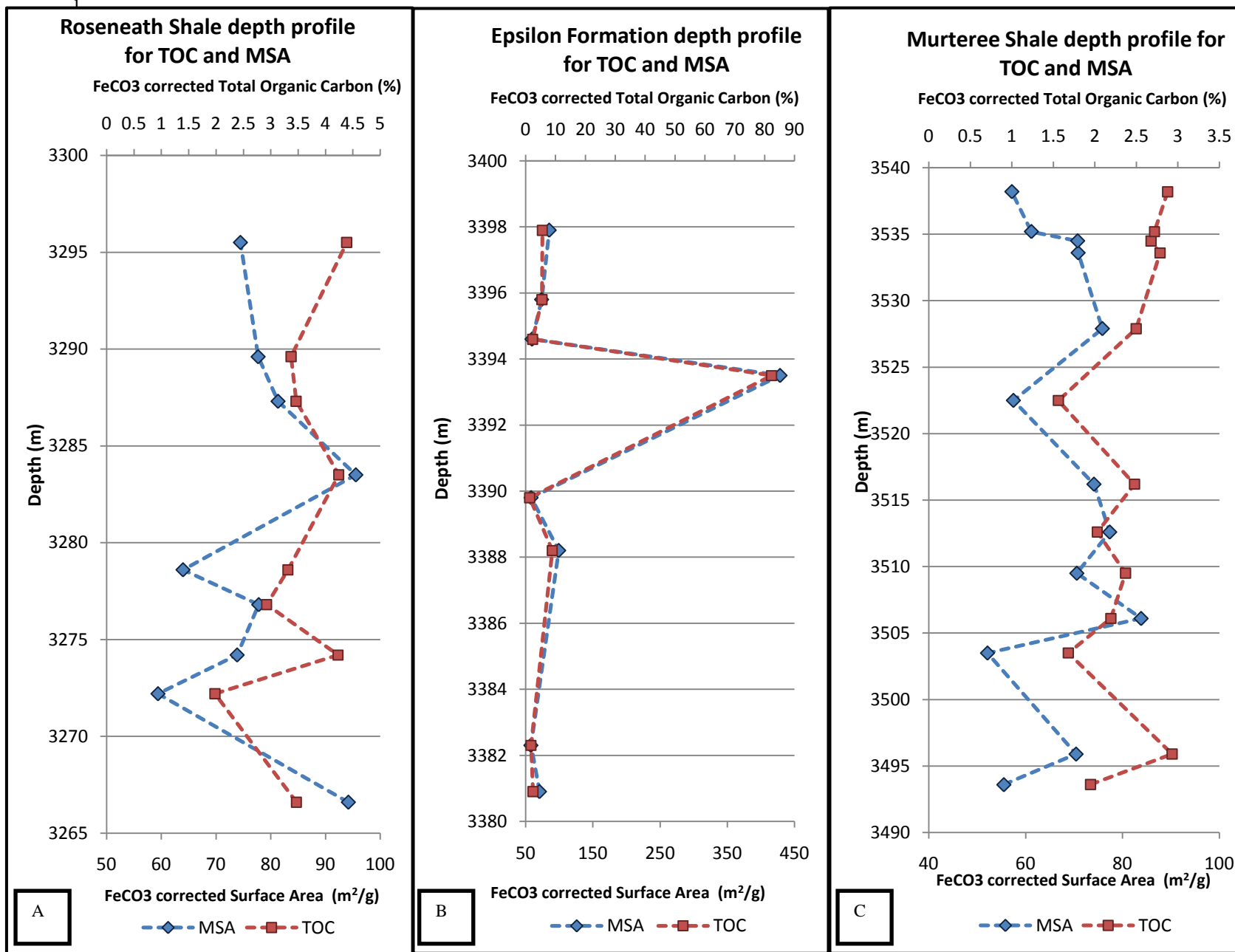
Figure 18: Depth vs mineral surface area (MSA) and TOC cross plots for selected samples within the Roseneath, Epsilon and Murteree formations within Encounter 1. (a) MSA and TOC variations within the Roseneath Shale. No coupling between MSA and TOC is apparent. (b) MSA and TOC variations appear strongly coupled within the Epsilon Formation. The highest recorded surface area is recorded within this formation (428.48m^2/g), associated with an 88% TOC coal. (c) MSA and TOC variations within the Murteree Shale. Much like for the Roseneath Shale, no coupling between MSA and TOC is apparent. For TOC-MSA depth profiles for Vintage Crop 1, see Appendix C
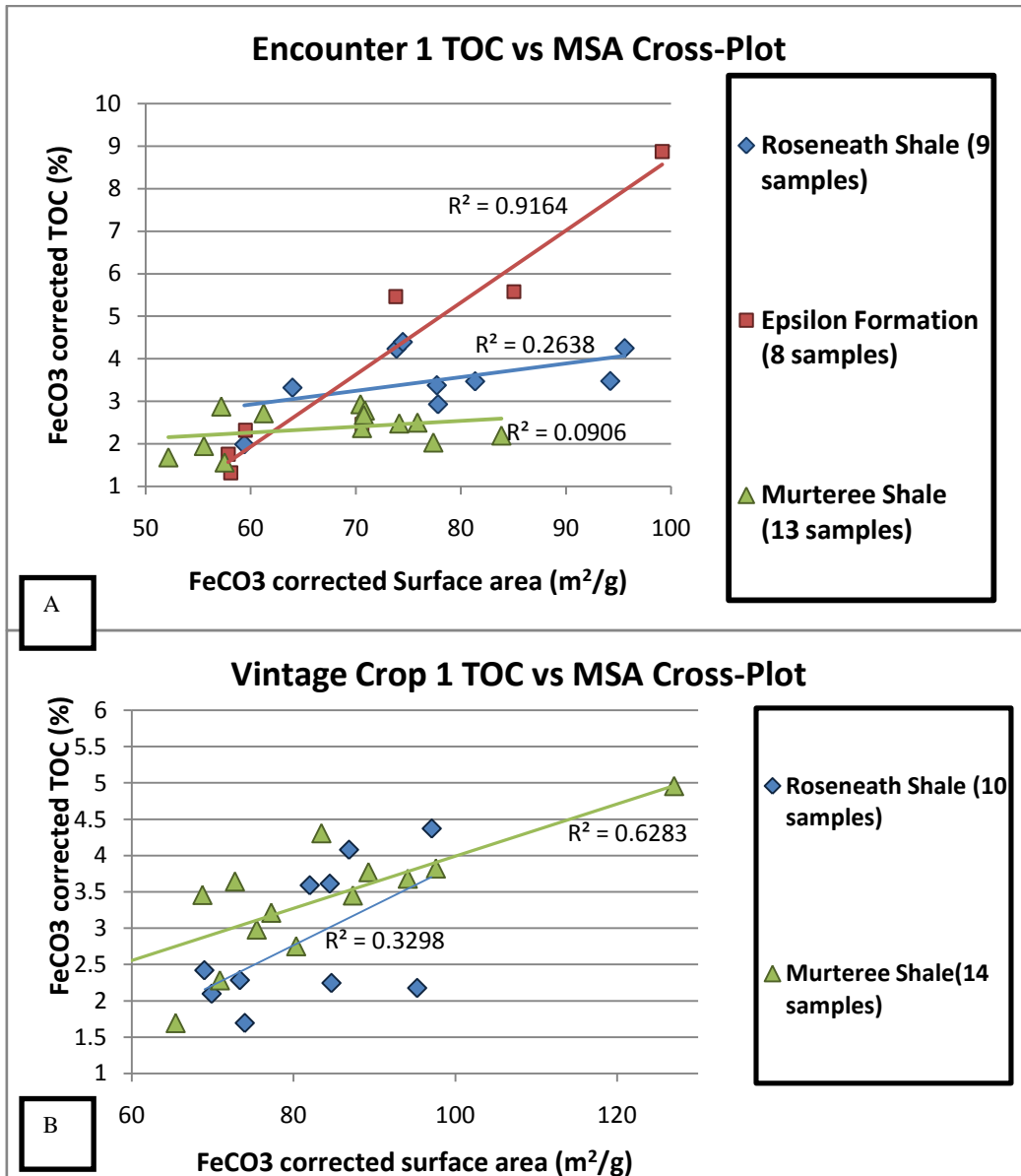
Figure 19: TOC-MSA cross plots for Encounter 1 and Vintage Crop 1 cores. (a) The TOC-MSA cross plot indicates little to know correlation between organic carbon content and mineral surface area within the Roseneath and Murteree Shales, while a strong $R^2 = 0.91$ correlation exists within the Epsilon Formation. Note that for the purposes of this cross plot, to Epsilon coal sample with anomalously high MSA was omitted, to prevent skewing of the data set. (b)The TOC-MSA cross plot for Vintage Crop 1 again indicates little to no correlation between organic carbon content and the mineral surface area for the Roseneath and Murteree Shales. As the Epsilon Formation was not cored for Vintage Crop 1, it is unclear of how TOC-MSA would correlate in a less mature sample.

A comparison between figures a and b suggests sample maturity may play some role in determining the TOC MSA correlation, with higher R^2 values for Vintage Crop 1 samples in comparison to Encounter 1. However, this may simply be a function of the small sample size for the data set.
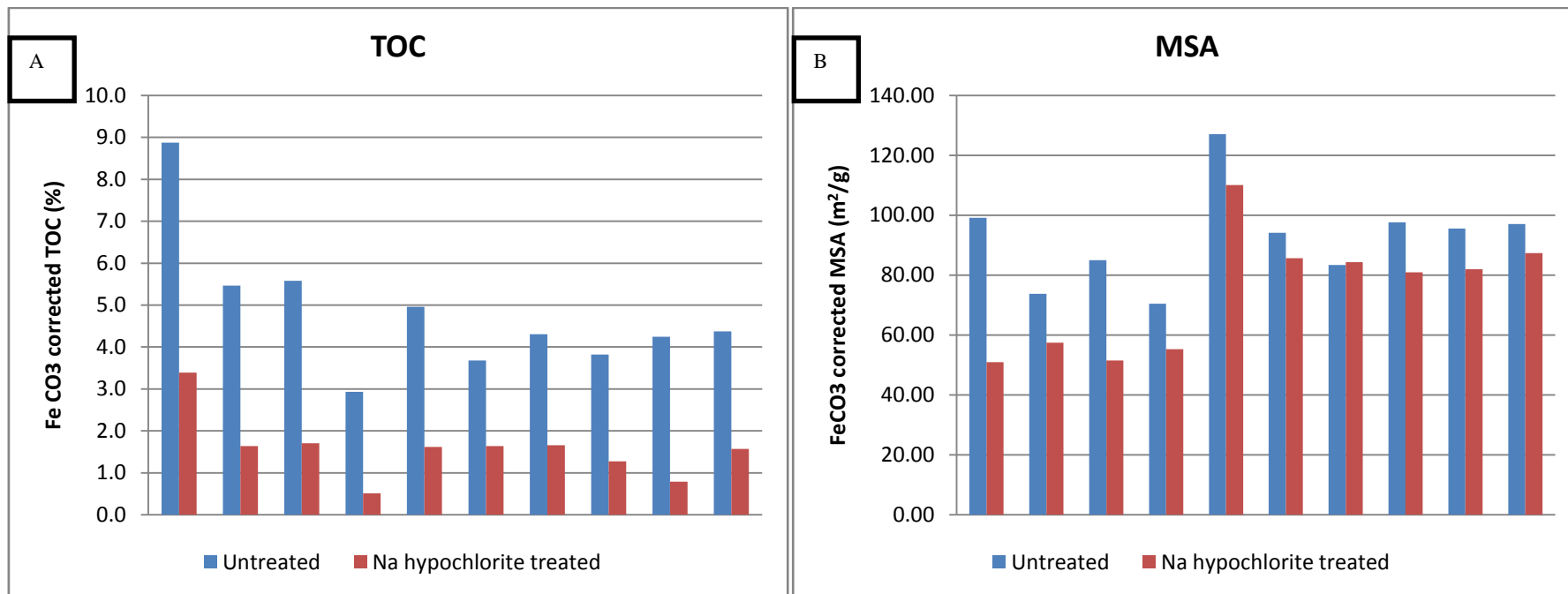
Figure 20: Histograms showing the difference in total organic carbon and MSA before and after treatment with sodium hypochlorite to remove organic matter. (a) TOC comparison between samples treated with sodium hypochlorite to remove organic matter (Na hypochlorite treated) and samples that were untreated. TOC was reduced between 56 and 81%. (b) MSA comparison between organic matter removed samples (Na hypochlorite treated) and samples that were untreated. MSA was found to be consistently reduced in organic matter removed samples, suggesting a role for organic matter in EGME sorption. The difference in MSA between Na hypochlorite treated and untreated samples varied between a +1% increase in MSA to a 49% reduction, with an average of 20% reduction.
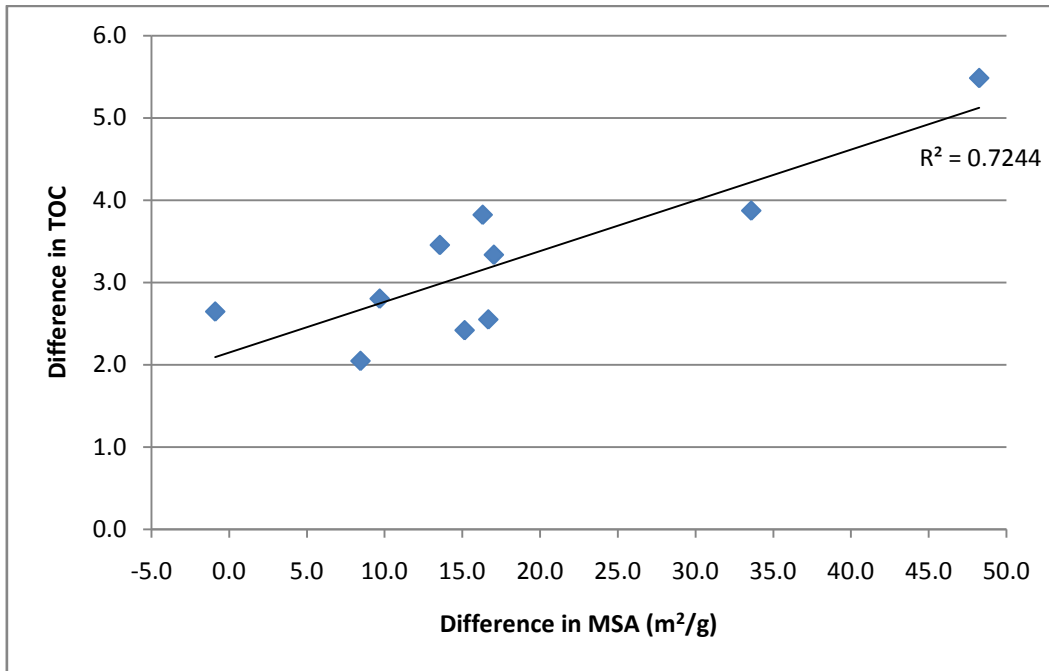
Figure 21: Cross plot of difference in TOC against the difference in MSA, which shows that a correlation exists between the amount of organic matter that has been removed from coaly shales and the reduction in MSA that is observed.

DISCUSSION

Modes of organic matter occurrence within the REM

A number of potential mechanisms were suggested to explain the presence of organic matter within the REM. Based on a combination of BSEM micron-scale imaging and geochemical analysis it is propose 2 mechanisms account for organic matter enrichments between 1-8%.

The first mechanism suggests that detrital plant material has been transported into the basin from the hinterland by fluvial or aeolian processes. The nature of a dominantly detrital plant source of organic matter is supported by direct observation of 20-50μm sized tabular and spherical organic matter particles interpreted to be spores and woody plant material, and by its gas prone to inert geochemical nature when analysed using the RockEval technique. Independent organic petrography and geochemistry conducted on samples of the REM section further support these observations. Weatherford Laboratories (2012) described samples from Vintage Crop 1 as containing organic matter dominated by inertinite and vitrinite, with a significantly lower algal input, based on shape, reflectance and fluorescence descriptors, while Smyth (1985) described similar geochemical characteristics from rock chip samples from the REM within the Patchawarra Trough. While inertinite properties can be reached through different pathways (either by initial OM properties, oxidation or recurrent hydrocarbon generation events), the presence of vitrinite is conclusive as it can only be explained by the thermal maturation of woody plant material (Dyrkacz & Horwitz 1982).

The second mechanism for organic matter occurence within the REM is associated with migration processes. This mechanism is supported by observations of organic matter residing within the intergranular pore space between detrital grains, the mineral contact defined shapes of the organic matter, and evidence of grain coating features indicative of migrating hydrocarbon (14a). The presence of a migrated component suggests an organic matter source other than gas prone woody and higher plant derived organic material, though it is unclear from backscattered microscopy if this is locally sourced or the result of larger scale migration. RockEval analysis of the organic matter reveals values for the free gas component to be low (0.05-0.58mgHC/gTOC), suggesting that the migrated phase, while present, does not represent a dominant component across the whole of the REM. Alternatively, these pore-filling organics may represent a refractory hydrocarbon component (bitumen) left behind during a migration event.

Based on data presented within this study, deposition of a secondary, refractory form of organic matter, such as eroded coals and shales, does not appear to represent a dominant form of organic matter. Despite the samples having low hydrogen index values indicative of this organic matter form, and the presence of coal flakes observed at the core scale, large lithified organic grains were not present in large enough quantities using BSEM to warrant suggestion that this represents the dominant mechanism. A bioproductivity driven mechanism for organic matter enrichment is not supported by the data either, with petrographic relations showing pore filling organic matter and detrital plant material, and geochemical analyses indicating a low hydrogen index not typical of algal material. Low HI values cannot be explained by thermal maturity because they are characteristic of organic matter in the Vintage Crop 1 core that has %Ro values

indicative of mid to late oil window. However, the observation of a rare fossil algal cell indicates algal material did constitute a minor component of pelagic organic matter. This is consistent with previous work by Smyth (1985), which describes the presence of a minor algal component within REM sediments otherwise dominated by plant detritus with the use of organic petrography.

Low TOC-MSA correlations support observations from BSEM that clays within the REM are dominated by diagenetic kaolinite and large detrital micas which would not provide the required surface area for preservation. While minor amounts of detrital illite clays are present, and diagenetic illite is observed through BSEM and clay XRD, these were not evidently observed to be associated with organic carbon peaks using EDAX, leading to the conclusion that clay mineral associations are not a dominant influence on organic matter preservation within the REM.

The laminated and rhythmic nature of organic siltstone deposition within the REM interval implies a cyclic depositional control. Observations from BSEM and microprobe imaging indicates organic matter is dominantly associated with laminations that are fine grained, have smaller pore spaces and low siderite abundance. These laminations are highlighted in core observations and in BSEM by the presence of siderite, which is dominantly associated with coarser siltstone laminations.

Detailed sedimentological core descriptions support the suggestion that the cyclic pattern is the product of spring flooding events. Spring floods carry variable amounts of detrital quartz, micas, clays and organic matter from the hinterland to the basin on a

biannual basis. Due to their strong energy currents and periodic nature, rivers transport sediments as a chaotic mixture of particles, depositing them in the basin as mass flows of poorly sorted, variably grain sized sediments, while creating plumes of fine-grained sediments that extend in the water surface settling down and mixing slowly with the organic matter present in the water column (i.e spores and fragments of plants or wood) during the quiescent periods of river activity. Therefore, sediment cycles associated to these spring floods would be characterized by a poorly mature and poorly sorted detrital quartz grains, clays and micas at the base, direct product of mass flows deposits, grading to fine-grained, well mature and sorted clays mixed with organic matter particles settling down from the water column. While no spectral analyses were conducted to determine cycle length, the spring flood model represents a viable depositional mechanism for this setting due to the accuracy in predicting zones of coarse and fine-grained cyclic zones.

Diagenesis

Diagenesis within the REM plays a significant role in controlling porosity and permeability, which could prove a significant control on hydrocarbon distribution, particularly given the observation that an abundance of organic matter within REM samples resides within intergranular pore spaces. Siderite, illite and kaolinite, identified both through BSEM and bulk powder and clay fraction XRD, all occur as the primary pore occluding cement phases within the REM. Observed phase relationships centre particularly around the timing of siderite precipitation.

Siderite precipitation typically requires low sulphide abundance, high dissolved carbonate concentrations, neutral pH and a high ratio of Fe^{2+}/Ca^{2+}, such as those found in lake and swamp deposits (Berner 1981, Bahrig 1989, Schulz-Rojahn 1991). A significant source of iron is also required. At least 2 separate phases of siderite precipitation were recognized within REM sediments, based on BSEM observations of Fe-rich microcrystalline and mixed Fe-Mg rich sparry siderite phases. The suggestion of multiple pulses of siderite development is supported by previous work, which suggest siderite precipitation occurred over a temperature range from 30 up to >100 degrees Celsius and from depths between 1 and 2km (Schulz-Rojahn 1991, Rezaee *et al.* 1997, Rezaee & Schulz-Rojahn 1998). However, isotopic analyses carried out in Vintage Crop 1 samples suggests a higher temperature for siderite precipitation with oxygen values ranging from -16.45‰ and -13.96‰. A possible explanation for the depleted isotopic values is that isolated siderite phases were not captured, but rather there is mixing between the Fe-rich and Fe/Mg siderite end members. Alternatively, the fluids from which the siderite precipitated may have originally been more depleted in O^{18} than anticipated. O^{18} isotope values are influenced by changes in rainfall sources, fluvial influx, groundwater interactions and ambient temperature (Schwalb & Dean 2002, Leng & Marshall 2004, Yansa *et al.* 2007), with lake environments being particularly sensitive, commonly showing variations of several ‰ (Talbot 1990). Given the interpretation that microcrystalline siderite is dominantly single phase, and associated with pore occlusion, this would likely represent the initial sideritic phase, as later fluids would be unable to permeate through these carbonate altered sediments. However, it is difficult based on this model to explain the presence of migrated hydrocarbons. If hydrocarbon migration post dates siderite precipitation, it is likely that the siderite

would have acted as local seals. Alternatively, if migrated hydrocarbon predated siderite emplacement, why then were organics not dominantly associated with the coarser siltstone fraction? One possible explanation is that siderite precipitation is facilitated by the breakdown of pre existing organic matter.

Phase relationships highlighted in figures 8f, and 15a-d indicate that sparry siderite has precipitated from the breakdown and replacement of organic matter, detrital micas and detrital and authigenic illite. While replacement of a detrital component cannot constrain much regarding timing of siderite precipitation, observations of diagenetic phases being replaced by another certainly can. Since authigenic illite typically develops within the oil window (Eslinger & Pevear 1988), it suggests that replacement of diagenetic illite by siderite precipitation is the result of an oil window or post oil window form event. If this is the case, sparry siderite precipitation may have been synchronous with or post dated hydrocarbon migration.

As mentioned previously, kaolinite becomes unstable and undergoes illitisation at temperatures between 120-140 degrees Celsius (Hurst & Kunkle 1985, Lanson *et al.* 2002) and must therefore represent a later diagenetic feature. Formation of kaolinite is likely the result of breakdown of detrital feldspars and micas, as evidenced by 20-50 micron pockets of pervasive kaolinite growth not associated with the intergranular pore space, and the absence of feldspars in XRD. Phase relationships indicating timing for chlorite development were not observed within the studied samples, however previous studies have suggested a late oil window-early dry gas window origin for chlorite development (Schulz-Rojahn 1991).

Mineral Surface Area

The strong TOC-MSA correlation within the Epsilon Formation , despite no observed clay-organic association, coupled with anomalously high MSA values associated with coal samples ($428.48 m^2/g$), implies a secondary control of total organic carbon on EGME sorption. This is further supported by comparisons with organic removed samples, which showed up to 46% reduction in MSA when between 56-81% of organic carbon is removed. However, due to the inert nature of the organic matter within the REM, samples were more resistant to sodium hypochlorite treatment, resulting in less organic carbon removal than expected. Subsequently, the full effect of organic matter removal on surface area calculation could not be ascertained.

The premise of the EGME test is that a higher MSA indicates a greater abundance of smectites, which have the capability of bonding to and preserving organic matter (Tiller & Smith 1990). The assumption with this method however, is that EGME sorbs only to the silicate fraction of the sample. It appears however, that EGME does not sorb solely to the surface of the silicate fraction, but also to the surface of organics, which may be resulting in an autocorrelation between TOC and MSA. This is particularly true in organic sediments dominated by higher order plant derived material, such as in coals, where a preservational relationship with smectites does not exist. Organic matter, and particularly coal related organic matter, has long been reported to have very high surface areas (Gan *et al.* 1972), which would make them more than capable receptacles of significant proportions of EGME. In fact, in soil organic matter studies, ethylene glycol (EG) has been utilised as a proxy for estimating the surface area provided by organic matter for this same reason (Chiou *et al.* 1990). However, the fact that the TOC-

MSA relationship does not exist for the lower TOC formations the Roseneath and Murteree shales implies that the abundance of TOC plays an important role in defining the TOC-MSA relationship.

Permian Gas shows within the Nappamerri Trough

Evidence of high TOC (1-8%), low free gas (S1) and low hydrocarbon potential (S2) of the REM section suggests that the organic matter which accounts for the high organic carbon content is not a viable source for significant hydrocarbon generation, most likely the reflection of a high proportion of inertinite. As a result, significant gas shows with the REM appear to be the result of upward migration as part of a basin centred gas accumulation, as put forward by Hillis *et al.* (2001), rather than the more typical process of self sourcing in unconventional plays. Coals within the Patchawarra Fm have long been considered the major source rock for Permian aged Cooper Basin sediments (Alexander *et al.* 1998, Boucher 2001). and likely represent the hydrocarbon source in this instance. The Patchawarra coals, while enriched in inertinite when compared with other coal source rocks, have still shown a substantial capacity for hydrocarbon generation (Hunt and Smyth 1989).

The Roseneath and Murteree shales represent poor quality hydrocarbon reservoirs dominated by poorly sorted, compositionally immature sediments rich in detrital phyllosilicates and diagenetic clays and carbonates. Cyclically deposited fine grained, low porosity sediments may act as local seals preventing hydrocarbon migration, with the impact of pore occlusion as a result of clay and carbonate diagenesis further exacerbating the low porosity and permeability. While a secondary phyllosilicate

porosity it is common, BSEM cannot determine how interconnected these zones are. The Epsilon formation is characterized by deposition of high porosity sandstone dominated sections that may have served as suitable hydrocarbon reservoirs. However, precipitation of diagenetic clays and siderite during burial diagenesis has occluded porosity turning them into possible permeability barriers for hydrocarbon migration. The key to prospectivity in the REM may therefore be the timing of diagenetic pore filling seals relative to the timing of charge migration.

CONCLUSIONS

Organic carbon concentrations between 1 and 8% within the REM section are controlled by detrital influxes of higher order plant material and enrichment through a migrated hydrocarbon component. The abundance of higher order plant material and low S2 fractions as shown by RockEval, imply poor generative potential, which would suggest gas shows within the REM are migration driven as opposed to self sourced.

Diagenetic clays and siderite control the majority of porosity within the REM, both through occlusion of intergranular pore space and as a result of secondary porosity created by the phyllosilicate fraction, although based on BSEM alone it cannot be determined if this phyllosilicate porosity is connected. Siderite plays a particularly important role within the REM, occurring within cyclic laminations with coarser siltstone fractions as a pore occluding phase that limit migration potential.

In summary, organic matter within the REM is associated to detrital influxes of higher order plant material and enrichment through a migrated hydrocarbon component. Due to

the inert nature of the detrital organic matter, gas shows within the REM are the result of upward migration from lower source beds controlled by the presence of local depositional seals and pore occluding diagenetic clays and carbonates. The key to prospectivity in the REM may therefore be the timing of diagenetic pore filling seals relative to the timing of charge migration.

ACKNOWLEDGMENTS

12

REFERENCES

ALEXANDER E. M., GRAVESTOCK D., JENSEN-SCHMIDT B., HIBBURT J. & DREXEL J. 1998. *The petroleum geology of South Australia. Vol. 4: Cooper Basin* (South Australia. Department of Primary Industries and Resources. Report Book, 98, Vol. 9).

ARTHUR M. A. & SCHLANGER S. O. 1979. Cretaceous" oceanic anoxic events" as causal factors in development of reef-reservoired giant oil fields. *AAPG Bulletin* **63**, 870-885.

BAHRIG B. 1989. Stable isotope composition of siderite as an indicator of the paleoenvironmental history of oil shale lakes. *Palaeogeography, Palaeoclimatology, Palaeoecology* **70**, 139-151.

BERNER R. A. 1981. A new geochemical classification of sedimentary environments. *Journal of Sedimentary Research* **51**, 359-365.

BERNER R. A. & CANFIELD D. E. 1989. A new model for atmospheric oxygen over Phanerozoic time. *American Journal of Science* **289**, 333-361.

BOEGLIN J.-L. & PROBST J.-L. 1998. Physical and chemical weathering rates and CO_2 consumption in a tropical lateritic environment: the upper Niger basin. *Chemical Geology* **148**, 137-156.

BOHACS K. M., GRABOWSKI G., CARROLL A. R., MANKIEWICZ P. J., MISKELL-GERHARDT K. J., SCHWALBACH J., WEGNER M. B. & SIMO J. 2005. Production, destruction, and dilution-the many paths to source-rock development. *SPECIAL PUBLICATION-SEPM* **82**, 61.

BOUCHER R. K. 2001. Analysis of seals of the Roseneath and Murteree Shales, Cooper Basin, South Australia. *Primary Industries and Resources SA*.

CARROLL A. R. & BOHACS K. M. 2001. Lake-type controls on petroleum source rock potential in nonmarine basins. *AAPG Bulletin* **85**, 1033-1053.

CHIOU C. T., LEE J. F. & BOYD S. A. 1990. The surface area of soil organic matter. *Environmental science & technology* **24**, 1164-1166.

COLE T. & SHAW H. 1983. The nature and origin of authigenic smectites in some recent marine sediments. *Clay minerals* **18**, 239-252.

CROWELL J. C. & FRAKES L. A. 1971. Late Paleozoic glaciation: Part IV, Australia. *Geological Society of America Bulletin* **82**, 2515-2540.

DYRKACZ G. R. & HORWITZ E. P. 1982. Separation of coal macerals. *Fuel* **61**, 3-12.

EIA U. 2011. Review of emerging resources: US shale gas and shale oil plays. *EIA, Ed*, 4.

EMERSON S. & HEDGES J. 1988. Processes controlling the organic carbon content of open ocean sediments. *Paleoceanography* **3**, 621-634.

ESLINGER E. & PEVEAR D. R. 1988. *Clay minerals for petroleum geologists and engineers*. Society of Economic Paleontologists and Mineralogis ts.

ESPITALIE J., MADEC M., TISSOT B., MENNIG J. & LEPLAT P. 1977. Source rock characterization method for petroleum exploration. *Offshore Technology Conference*.

GAN H., NANDI S. & WALKER JR P. 1972. Nature of the porosity in American coals. *Fuel* **51**, 272-277.

GATEHOUSE C. 1972. Formations of the Gidgealpa Group in the Cooper Basin. *Australasian Oil and Gas Review* **18**, 10-15.

GRAHAM S., BRASSELL S., CARROLL A., XIAO X., DEMAISON G., MCKNIGHT C., LIANG Y., CHU J. & HENDRIX M. 1990. Characteristics of Selected Petroleum Source Rocks, Xianjiang Uygur Autonomous Region, Northwest China (1). *AAPG Bulletin* **74**, 493-512.

HEDGES J. I. & KEIL R. G. 1995. Sedimentary organic matter preservation: an assessment and speculative synthesis. *Marine Chemistry* **49**, 81-115.

HILL A., MENPES S., BACKE G., KHAIR H. & SIASITORBATY A. 2011. Shale gas prospectivity in South Australia. *APPEA Journal* **51**.

HILLIS R., MORTON J., WARNER D. & PENNEY R. 2001. Deep basin gas: A new exploration paradigm in the Nappamerri Trough, Cooper Basin, South Australia. *APPEA Journal* **41**, 185-200.

HORSFIELD B., CURRY D., BOHACS K., LITTKE R., RULLKÖTTER J., SCHENK H., RADKE M., SCHAEFER R., CARROLL A. & ISAKSEN G. 1994. Organic geochemistry of freshwater and alkaline lacustrine sediments in the Green River Formation of the Washakie Basin, Wyoming, USA. *Organic Geochemistry* **22**, 415-440.

HURST V. J. & KUNKLE A. C. 1985. Dehydroxylation, rehydroxylation, and stability of kaolinite. *Clays Clay Miner* **33**, 1-14.

ISAACS C. 1987. Sources and deposition of organic matter in the Monterey Formation, south-central coastal basins of California.

KAPEL A. 1972. The Geology of the Patchawarra area, Cooper Basin. *APPEA Journal* **6**, 53-56.

KEIL R. G., MONTLUÇON D. B., PRAHL F. G. & HEDGES J. I. 1994. Sorptive preservation of labile organic matter in marine sediments.

KENNEDY M. J., PEVEAR D. R. & HILL R. J. 2002. Mineral surface control of organic carbon in black shale. *Science* **295**, 657-660.

KENNEDY M. J. & WAGNER T. 2011. Clay mineral continental amplifier for marine carbon sequestration in a greenhouse ocean. *Proceedings of the National Academy of Sciences*.

KLEMME H. & ULMISHEK G. F. 1991. Effective petroleum source rocks of the world: stratigraphic distribution and controlling depositional factors (1). *AAPG Bulletin* **75**, 1809-1851.

KUANG K. 1985. History and style of Cooper-Eromanga Basin structures. *Exploration Geophysics* **16**, 245-248.

LANSON B., BEAUFORT D., BERGER G., BAUER A., CASSAGNABERE A. & MEUNIER A. 2002. Authigenic kaolin and illitic minerals during burial diagenesis of sandstones: a review. *Clay minerals* **37**, 1-22.

LENG M. J. & MARSHALL J. D. 2004. Palaeoclimate interpretation of stable isotope data from lake sediment archives. *Quaternary science reviews* **23**, 811-831.

LINDSAY J. 2000. Source rock potential and algal-matter abundance, Cooper Basin, South Australia. *PIRSA Report Book* **32**.

MAVROMATIDIS A. 2008. Two layer model of lithospheric compression and uplift/exhumation in an intracratonic setting: an example from the Cooper–Eromanga Basins, Australia. *International Journal of Earth Sciences* **97**, 623-634.

MAYER L. M. 1994. Surface area control of organic carbon accumulation in continental shelf sediments. *Geochimica et Cosmochimica Acta* **58**, 1271-1284.

MEYERS P. A. & ISHIWATARI R. 1993. Lacustrine organic geochemistry—an overview of indicators of organic matter sources and diagenesis in lake sediments. *Organic Geochemistry* **20**, 867-900.

PASSEY Q., BOHACS K., ESCH W., KLIMENTIDIS R. & SINHA S. 2010. From Oil-prone source rock to gas-producing shale reservoir-geologic and petrophysical characterization of unconventional shale gas reservoirs. *International Oil and Gas Conference and Exhibition in China*.

PEARSON V. K., SEPHTON M. A., KEARSLEY A. T., BLAND P. A., FRANCHI I. A. & GILMOUR I. 2002. Clay mineral-organic matter relationships in the early solar system. *Meteoritics & Planetary Science* **37**, 1829-1833.

POPPE L., PASKEVICH V., HATHAWAY J. & BLACKWOOD D. 2001. A laboratory manual for X-ray powder diffraction. *US Geological Survey Open-File Report* **1**, 1-88.

POWELL C. & VEEVERS J. J. 1987. Namurian uplift in Australia and South America triggered the main Gondwanan glaciation. *Nature* **326**, 177-179.

RANSOM B., KIM D., KASTNER M. & WAINWRIGHT S. 1998. Organic matter preservation on continental slopes: importance of mineralogy and surface area. *Geochimica et Cosmochimica Acta* **62**, 1329-1345.

REZAEE M., LEMON N. & SEGGIE R. 1997. Tectonic fingerprints in siderite cement, Tirrawarra Sandstone, southern Cooper Basin, Australia. *Geological Magazine* **134**, 99-112.

REZAEE M. R. & SCHULZ-ROJAHN J. 1998. Application of Quantitative Back-Scattered Electron Image Analysis in Isotope Interpretation of Siderite Cement: Tirrawarra Sandstone, Cooper Basin, Australia. *Carbonate Cementation in Sandstones: Distribution Patterns and Geochemical Evolution*, 461-481.

RITTS B. D., HANSON A. D., ZINNIKER D. & MOLDOWAN J. M. 1999. Lower-Middle Jurassic nonmarine source rocks and petroleum systems of the northern Qaidam basin, northwest China. *AAPG Bulletin* **83**, 1980-2005.

SAGEMAN B. B., MURPHY A. E., WERNE J. P., VER STRAETEN C. A., HOLLANDER D. J. & LYONS T. W. 2003. A tale of shales: the relative roles of production, decomposition, and dilution in the accumulation of organic-rich strata, Middle–Upper Devonian, Appalachian basin. *Chemical Geology* **195**, 229-273.

SCHULZ-ROJAHN L. 1991. Origin, evolution and controls of Permian reservoir sandstones in the southern Cooper Basin, South Australia. University of Adelaide (unpubl.).

SCHWALB A. & DEAN W. E. 2002. Reconstruction of hydrological changes and response to effective moisture variations from North-Central USA lake sediments. *Quaternary science reviews* **21**, 1541-1554.

SHERROD L., DUNN G., PETERSON G. & KOLBERG R. 2002. Inorganic carbon analysis by modified pressure-calcimeter method. *Soil Science Society of America Journal* **66**, 299-305.

SMITH D. G. & GRIFFITHS C. M. 1999. Undiscovered Resources of the Cooper Basin (SA). *Primary Industry and Resources, South Australia Stratigraphy Australia*.

SMITH M. G. & BUSTIN R. M. 1998. Production and preservation of organic matter during deposition of the Bakken Formation (Late Devonian and Early Mississippian), Williston Basin. *Palaeogeography, Palaeoclimatology, Palaeoecology* **142**, 185-200.

SMYTH M. 1985. The relationship between coals and dispersed organic matter in associated sediments in four basins in central Australia. *University of Wollongong Thesis Collection*, 2119.

TALBOT M. 1990. A review of the palaeohydrological interpretation of carbon and oxygen isotopic ratios in primary lacustrine carbonates. *Chemical Geology: Isotope Geoscience Section* **80**, 261-279.

THIRY M. 2000. Palaeoclimatic interpretation of clay minerals in marine deposits: an outlook from the continental origin. *Earth-Science Reviews* **49**, 201-221.

THORNTON R. & HUDSON H. 1979. *Regional stratigraphic analysis of the Gidgealpa Group, southern Cooper Basin, Australia* (Vol. 49). Department of Mines and Energy, Geological Survey of South Australia.

TILLER K. & SMITH L. H. 1990. Limitations of EGME retention to estimate the surface area of soils. *Soil Research* **28**, 1-26.

TISSOT B., DEROO G. & HOOD A. 1978. Geochemical study of the Uinta Basin: formation of petroleum from the Green River formation. *Geochimica et Cosmochimica Acta* **42**, 1469-1485.

TYSON R. 2001. Sedimentation rate, dilution, preservation and total organic carbon: some results of a modelling study. *Organic Geochemistry* **32**, 333-339.

VEEVERS J. J. 2006. Updated Gondwana (Permian–Cretaceous) earth history of Australia. *Gondwana Research* **9**, 231-260.

WEISSERT H. & MOHR H. 1996. Late Jurassic climate and its impact on carbon cycling. *Palaeogeography, Palaeoclimatology, Palaeoecology* **122**, 27-43.

WILSON M. 1999. The origin and formation of clay minerals in soils: past, present and future perspectives. *Clay minerals* **34**, 7-7.

YANSA C. H., DEAN W. E. & MURPHY E. C. 2007. Late Quaternary paleoenvironments of an ephemeral wetland in North Dakota, USA: relative interactions of ground-water hydrology and climate change. *Journal of Paleolimnology* **38**, 441-457.

ZAHID S., BHATTI A., AHMAD KHAN H. & AHMAD T. 2007. Development of unconventional gas resources: stimulation perspective. *Production and Operations Symposium*.

APPENDIX A: DETAILED METHODS

1.1 Sampling and Preparation

Samples were collected from two cores (Encounter 1 and Vintage Crop 1) stored at the DMITRE core library in South Australia. Both cores were drilled within the Nappamerri Trough in the Cooper Basin (Figure 1) and intersected the REM interval; however this occurred at different depths and is reflected in their differing maturities (Table 1). Encounter 1 and Vintage Crop 1 were studied to ascertain the lithological, geochemical and diagenetic variability not only over a thermal gradient, but also for differing positions within the Cooper Basin.
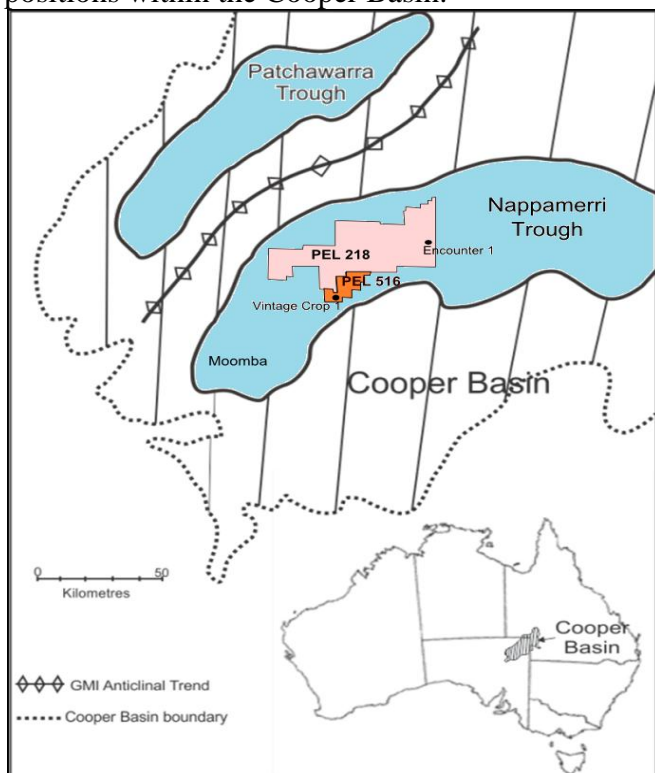
Figure 1: Location map showing the position of the Patchawarra and Nappamerri Troughs within the southern Cooper Basin, and within the Nappamerri Trough, the positions of Vintage Crop 1 and Encounter 1.

Table 1: Area and depth data for Vintage Crop 1 and Encounter 1

Core	Vintage Crop 1	Encounter 1
Petroleum Exploration Licence	516	218
Latitude	28˚ 30' 29.24˚S	27˚ 45' 16.6554˚S
Longitude	140˚ 41' 38.09˚E	140˚ 57' 30.6957˚E
Section of REM missing?	Epsilon Formation	None
Depth of core sampled	1840-1960m	3266-3542m
Approximate Maturity (Ro)	0.8-0.9%	3-4%

Both cores were logged to determine variation in lithology, sedimentary structures and diagenetic features within the REM, and a total of 138 samples were taken (60 from Encounter 1 and 64 from Vintage Crop 1) for a variety of geochemical analyses

(summarised in Table 2), as well as 20 thin sections. These analyses were supplemented with geochemical and petrophysical data from Encounter 1 and Vintage Crop 1 Well Completion reports, as well as organic petrography and geochemistry reports for Vintage Crop 1.

For samples requiring geochemical analysis, approximately 1 cm thick section of quarter core was taken and cleaned using deionised water and a wire brush to remove any potential contaminants. Samples were dried in a 40 degree oven overnight, and then crushed for 2 minutes using a Labtechnics LM 1/M vibrating mill fitted with a 100 g tungsten carbide mill head until the sample was a fine powder. Only half of each sample was crushed, so that other analyses, such as SEM, could be conducted if required.

Table 2: Summary of analyses conducted on Encounter 1 and Vintage Crop 1 samples.

Test	Number of Samples Run	
	Encounter 1	**Vintage Crop 1**
TOC	60	64
SRA	25	25
EGME	30	38
XRD	10	10
Gas Stable Isotopes	5	5
Siderite Stable Isotopes	N/A	8
Thin Section	10	10
SEM	5	5

High Resolution Sampling

As logging showed that variations in sediment composition was at a very fine resolution, a 15cm continuous quarter core section was taken from within the Roseneath shale interval of Vintage Crop 1. This core was cleaned and dried using the technique highlighted above, and then divided into 5mm bands with a chisel, utilising lamination planes as a guide. Each sample was then milled to a fine powder, again using the Labtechnics LM 1/M vibrating mill, and analysed for TOC variation.

1.2 Analyses
1.2.1 Pressure Calcimeter standard operating procedure
Cut micro-centrifuge tubes just above the 1.0ml mark.
Add 5 ml 4 M HCl/3% $FeCl_2$ solution to each glass vial.
Weigh out 200mg of each powdered sample into a cut micro-centrifuge tube and place this into a glass vial containing HCl acid. Make sure that the sample does not come into contact with the acid.
Weigh out 7 $CaCO_3$ standards and place into vials containing acid. $CaCO_3$ standard weights: 200mg, 150mg, 100mg, 75mg, 50mg, 25mg and 10mg
Cap all vials with a rubber stopper and a foil cap, and then crimp the foil using the hand crimper.
Once all samples and standards to be tested are capped shake each vial vigorously to ensure that all of the sample reacts with the acid.
Leave the vials sitting for half an hour, shaking them once more at the 15 min mark
Attach the hose and needle to the manometer

Tear out the centre of the aluminium cap on the first vial, pierce the rubber cap with the needle and record the maximum pressure vial. Repeat for all vials.

The weight and pressure of the standards and pressure recorded in each sample is then used to calculate the equivalent mass of CaCO3 in each sample (Figure 2). This value needs to be normalized to the exact mass of sample weighed into each centrifuge tube. This is most easily done in excel.
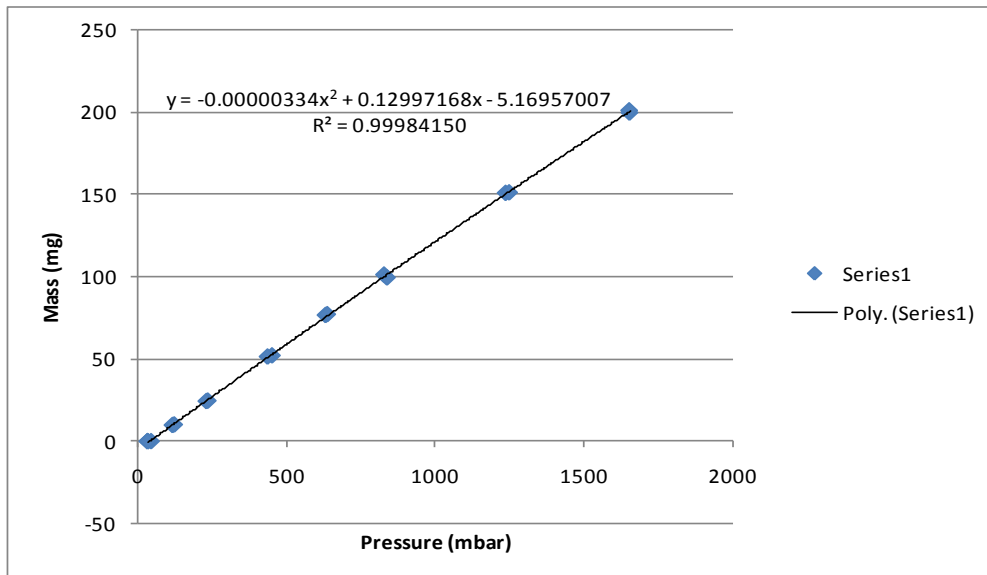
Figure 2: Polynomial fit for pressure vs mass using the calcium carbonate standards. The line equation is then used to back calculate inorganic carbon mass.

Convert %CaCO3 in each sample into % Inorganic carbon(IC)*

*Note- For step 11, % IC was calculated based on a conversion for siderite rather than for calcite.

Required Reagents: 4 M hydrochloric acid (HCl) with 3% (by weight) ferrous chloride ($FeCl_2 * 4H_2O$)

To prepare acid reagent mix 330 ml of concentrated (37%; 36.46 M) HCl with about 500 ml of water in a 1 L volumetric flask. Add 30 g ferrous chloride and dilute to total volume of 1 L.

1.2.2 EA and TOC calculation

To determine total carbon, powdered samples weighing approximately 7mg were analysed using a Perkin Elmer Series II CHNS/O Analyser 2400 running in CHN mode (only producing readings for carbon, hydrogen and nitrogen content). Calcium carbonate standards were run every ten samples to ensure data validity. Total organic carbon was then calculated by subtracting the inorganic carbon fraction, ascertained using pressure calcimeter testing, from total carbon.

1.2.3 X-ray Diffraction (XRD)

20 powdered samples were analysed for bulk mineralogy using a Bruker D8 Advance Diffractometer and Elemental Analyser. Samples were initially side loaded into a sample holder prior to analysis, ensuring the surface was flat and smooth. During

analysis, samples were exposed to Cu-Kα radiation at an angle of 3.5-45 degrees 2θ, with a step size of 0.005 degrees and a dwell time of 2 degrees per minute. Peaks were identified as particular mineral phases using Bruker Diffrac.Eva with Open Chrystallography Database software.

1.2.4 SRA artificial maturation tests

Artificial maturation was carried out using a Weatherford Source Rock Analyser (SRA). The Weatherford SRA standard operating procedure, as described below was followed.
Sample Preparation
1. If necessary, crush or pulverise the rock material, using a mortar and pestle, and pass through a 40-mesh sieve. Store the sample in the properly labelled envelope.
2. Take the cap off and empty the contents. Do not touch the crucible with your fingers. To avoid oil contamination from the analysts skin, either the crucibles must be handled with forceps, or the technician should wear latex or nitrile gloves. Contamination appears as hydrocarbon tracews.
3. Weigh out approximately 100mg of sample into the crucible.
4. Cap the crucible insert and place the crucible onto the auto sampler tray. An empty crucible is normally placed in position one in the autosampler tray, and position two is a daily calibration standard. Therefore the first sample crucible is placed in position three. Standards are run in positions 20, 40 60 etc *.
5. Go to the sequence editor and record all pertinent information such as sample weight, acquisition type (BLK, STD, TPH), as well as lithology, sample depth, depth measurement type and sample type if known.
6. Save data to a known file location.
6. Once all samples have been weighed, place the autosampler in the autosampler rack.
7. Check the instrument gas flow rates and make adjustments to gas flows if necessary.

Air	300 mL/min
Hydrogen	50 mL/min
Helium	50 mL/min

7. Initiate start up, and where promted load previously saved data file.

8. Autosampler will transfer the crucible from the autosampler tray to the SRA pedestal, which is raised, putting the sample into the 300°C oven. The sample is held isothermal at 300°C for 3 minutes. During this time, free hydrocarbons are are volatiilised and detected by the Flame Ionisation Detector (FID). These hydrocarbons are quantitatively detected and reported as S1 in milligrams of hydrocarbon per gram of rock.
9. After the isothermal period, the temperature is ramped up at 25°C/minute to 600°C. During this period of increasing temperature, organic hydrocarbons are generated from pyrolitic cracking of kerogen and other organics within the rock. The generated hydrocarbons are detected by the FID, labelled as S2 and again reported in milligrams of hydrocarbon per gram of rock. The temperature at which maximum release of hydrocarbons is released by cracking of organics (Tmax) is also recorded. Data is expressed both as a number (milligrams of hydrocarbon per gram of rock) and in the form of a pyrogram (Figure 2).
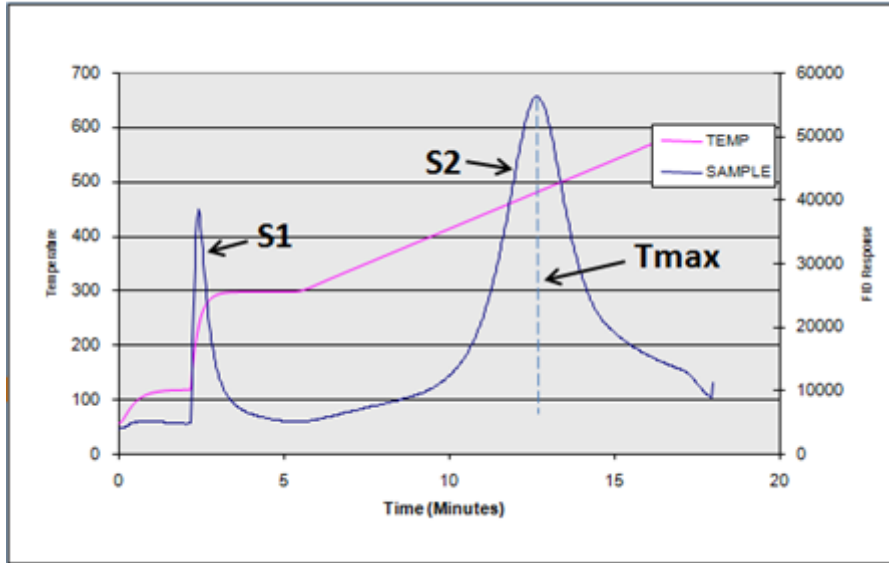
Figure 2: Typical pyrogram generated by the Weatherford SRA, showing S1, S2 and Tmax.

10. Calculate maturity (% Ro), kerogen type, hydrogen index (HI), oxygen index (OI) and production index based on the following equations, based on the procedure of Espitalie *et al.* (1977):

	Calculation
Maturity	0.0180* Tmax -7.16
Kerogen Type	Plot TOC vs S2
Hydrogen Index (mg HC/ g TOC)	S2* (100/TOC)
Oxygen Index (mg CO2/ g TOC)	S3 * (100/TOC)
Production Index (mg HC/ g rock)	S1/ (S1+S2)

* Note- In step 4, standards were run every 7 samples as opposed to every 20 to ensure reliable data was being produced.

1.2.5 Ethylene Glycol Monoethyl Ether (EGME) surface area measurement standard operating procedure

1. Calcium exchange

This step is required to ensure that the same cation (Ca) is on the exchange sites of all samples.

Weigh 1.1 g of sample into a 50 ml centrifuge tube

Add 15 ml of 1 M calcium chloride solution to each sample

Place samples on end-over-end shaker for 60 minutes

Remove samples from shaker and leave to settle overnight

Fill up to 50 ml mark with deionized water

Centrifuge samples for 10 minutes at 3000 rpm

Pour off the supernatant, be careful not to lose any sample

Add 50 ml deionized water to each sample, shake until all sample is suspended
Centrifuge samples for 10 minutes at 3000 rpm
Pour off supernatant
Repeat steps 7-9 once
Dry samples in oven at 40°C until dry
Once dry, homogenize each sample in agate mortar and pestle, return to centrifuge tubes
Store dried samples in oven or desiccator until weighed out for EGME analysis
2. EGME analysis
EGME method used here to obtain mineral surface areas follows the 'free surface' procedure of Tiller & Smith (1990).
Mark sample names on glass vials and plastic caps using a diamond pen
Record weight of the marked glass vials and caps using analytical balance to 5 decimal places
Weigh 1 g of oven dried, Ca-exchanged sample into the glass vials
Place uncapped vials with samples into oven ($110^{o}C$) for 48 hours to remove all sorbed water
Remove vials from oven and cap with the corresponding caps, as quickly as possible to avoid moisture absorption
IMPORTANT: Wear the white gloves under the nitrile gloves to avoid burning your fingers
Leave to cool in desiccator
Record the weight of the capped glass vials containing the dry samples
Place the vials into the plastic trays containing cardboard dividers – this will make it easier to place and remove the vials into the vacuum chamber
IMPORTANT: Remember to include 10 replicates of each of the standard clays, Ca-exchanged and oven dried like the samples.
Place 200g granular $CaCl_2$ and 40 ml EGME, in separate containers, into the sealed vacuum chamber
In the fume hood, add 1 ml of EGME to each sample
Place the uncapped vials containing the slurries in the sealed vacuum chamber and evacuate the chamber using the vacuum pump for 10 minutes – check that the vacuum chamber door is properly sealed and that the vacuum is increasing
Leave the samples until they all look dry (8-10 days, depending on mineralogy)
IMPORTANT: Remember to release the vacuum <u>gently</u> or you will blow over the vials and create a huge mess.
Replenish the EGME and replace the CaCl2 in the vacuum chamber every few days. This is best done when the samples are removed for weighing. Evacuate the chamber again after you are done – pump for 10 minutes
IMPORTANT: Cap the vials as soon as you remove them from the vacuum chamber to minimize the amount of water that the samples absorb during the weighing process. Get someone to help you if you have a large number of samples, this will speed up the capping.
Once the samples have dried weigh them every two days until they have reached a constant weight. This can take up to two weeks.
1.2.6 Stable Isotopes
Carbon and oxygen isotopes siderite samples
Stable isotope analyses were conducted on 8 powdered Vintage Crop samples weighing ~0.8 mg by the University of Melbourne using continuous-flow isotope-ratio mass

spectrometry on an Analytical Precision AP2003. Samples were digested in 105% phosphoric acid at 70°C and mass spectrometric measurements were made on the evolved CO2 gas. Results were normalised to the Vienna Pee Dee Belemnite scale using internal working standards of Carrara Marble (NEW1 – Newcastle), which was cross-checked against the international standards NBS18 and NBS19. Mean analytical precision for δ18O and δ13C was 0.7‰ and 0.3‰ respectively.

1.2.7 Petrography
Thin section and SEM analysis was conducted on selected samples to examine variations in sediment composition at varying scales as a means of determining patterns of cyclicity. Sideritic samples, as well as fine scours were also chosen to better determine understand the role of diagenesis and porosity variation across the REM.
Thin sections
20 Representative core samples were sent to Prograding Rock Services and Pontifex & Associates Ltd for thin section preparation. Sections were cut to fit 27mm*46mm slides, polished to approximately 35 microns thick and treated with a double carbonate stain. These were then viewed using reflected and transmission light optical petrography on a Nikkon LV100 POL microscope at Adelaide Microscopy.
Scanning Electron Microscope (SEM) Imaging
10 Representative samples were selected and cut into blocks that could fit onto 1cm diameter stubs. These blocks were then glued to the stubs, ensuring that the face perpendicular to bedding was facing upward, using an epoxy resin. The surface was polished using 1000 and 1200 grit sand paper, and a finer polish was achieved using an Argon mill beam. Samples were carbon coated to reduce charge interference on sample imaging, and viewed using backscattered scanning electron microscopy on a FEI Quanta 450 scanning electron microscope at Adelaide Microscopy.

APPENDIX B: XRD DATA SUMMARY

Table showing the present mineral phases, based on bulk powder and clay fraction XRD, within selected REM samples. 'X' represents mineral presence within a sample, while '-' indicates a mineral was not present. Samples with N/A were not ran for XRD.

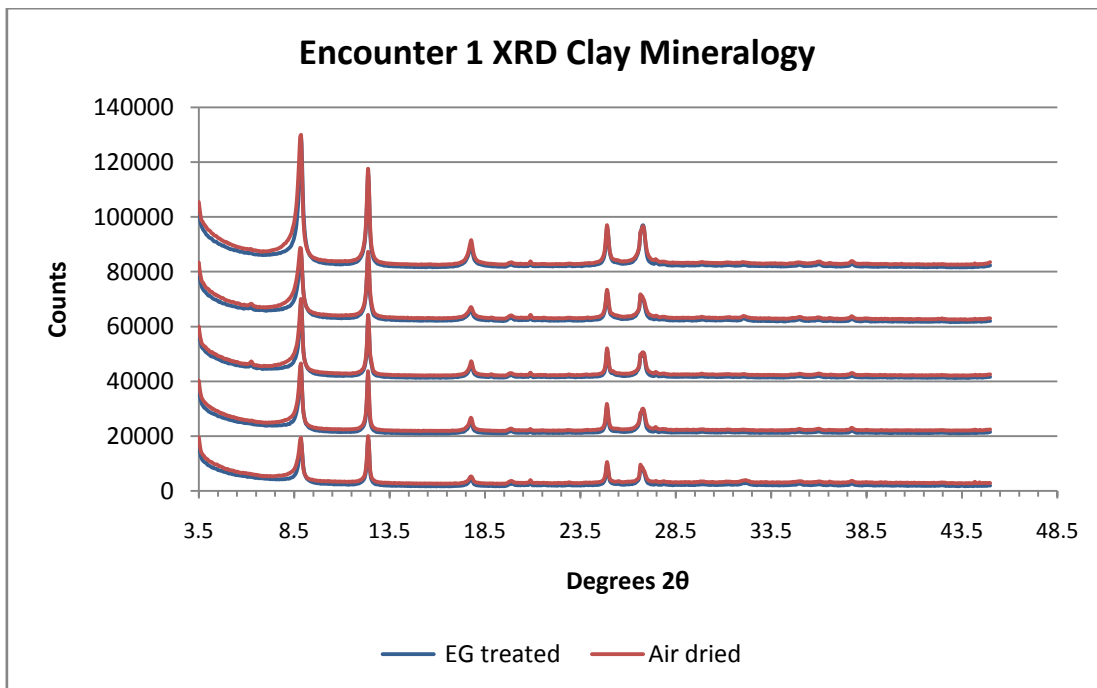| Sample	Bulk powder					Clay Fraction		
	Quartz	Muscovite	Fe Siderite	Mg Siderite	Kaolinite	Illite	Mixed Illite-smectite	Chlorite
824	X	X	X	X	X	X	X	-
775	X	X	X	X	X	N/A	N/A	N/A
806	X	X	X	X	X	N/A	N/A	N/A
795	X	X	X	X	X	X	X	-
796	X	X	X	X	X	X	X	-
791	N/A	N/A	N/A	N/A	X	X	X	-
772	N/A	N/A	N/A	N/A	X	X	X	-
228	X	X	X	X	X	X	X	-
245	X	X	-	-	X	N/A	N/A	N/A
250	X	X	X	X	X	X	X	-
271	X	X	X	X	X	N/A	N/A	N/A
278	X	X	X	X	X	X	X	X
232	N/A	N/A	N/A	N/A	X	X	X	-
241	N/A	N/A	N/A	N/A	X	X	X	X

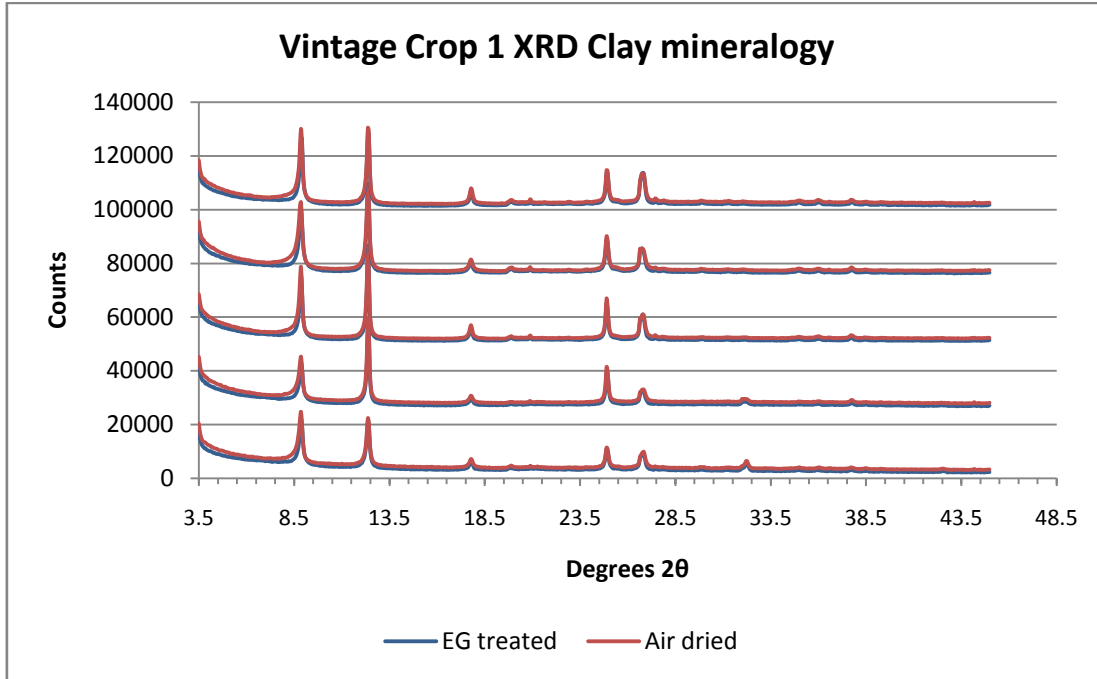Figure indicating present clay mineral peaks for REM samples for Encounter 1.

Figure indicating present clay mineral peaks for REM samples for Vintage Crop 1.

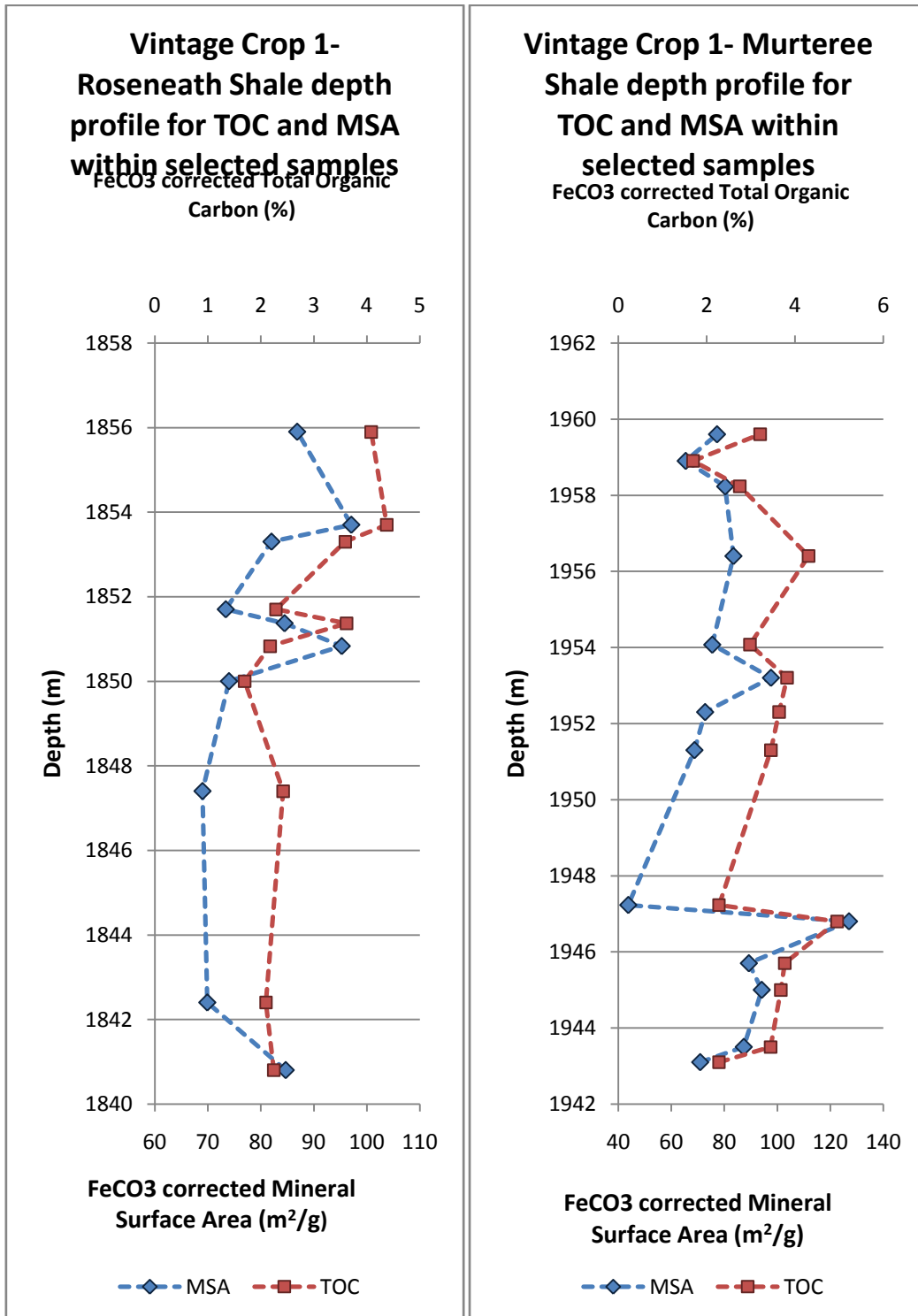## APPENDIX C: DEPTH PROFILE FOR TOC AND MSA IN VINTAGE CROP 1 SAMPLES

Figure showing depth profiles for the Roseneath and Murteree shales for Vintage Crop 1. Note the decoupling between TOC and MSA.